Powder Technology 400 (2022) 117190

Contents lists available at ScienceDirect

Powder Technology

journal homepage: www.elsevier.com/locate/powtec

Synthesis, stability, density, viscosity of ethylene glycol-based ternary hybrid nanofluids: Experimental investigations and model -prediction using modern machine learning techniques

Zafar Said [a,b,*], Nese Keklikcioglu Cakmak [c], Prabhakar Sharma [d], L. Syam Sundar [e], Abrar Inayat [a], Orhan Keklikcioglu [f], Changhe Li [g]

[a] Department of Sustainable and Renewable Energy Engineering, University of Sharjah, Sharjah, P. O. Box 27272, United Arab Emirates
[b] U.S.-Pakistan Center for Advanced Studies in Energy (USPCAS-E), National University of Sciences and Technology (NUST), Islamabad, Pakistan
[c] Department of Chemical Engineering, Faculty of Engineering, Sivas Cumhuriyet University, Sivas 58140, Turkey
[d] School of Engineering Sciences, Delhi Skill and Entrepreneurship University, Delhi 110089, India
[e] Department of Mechanical Engineering, College of Engineering, Prince Mohammad Bin Fahd University, Al Khobar 31952, Saudi Arabia
[f] Department of Mechanical Engineering, Faculty of Engineering, Erciyes University, Kayseri 38039, Turkey
[g] School of Mechanical and Automotive Engineering, Qingdao University of Technology, Qingdao 266520, China

ARTICLE INFO

Article history:
Received 25 November 2021
Received in revised form 25 January 2022
Accepted 9 February 2022
Available online 12 February 2022

Keywords:
Ternary nanocomposite
Hybrid nanofluid
Viscosity
Density
Artificial Neural Networks
Predictive modeling

ABSTRACT

A direct sol-gel technique was utilized to produce rGO-Fe_3O_4-TiO_2 ternary hybrid nanocomposites to produce ethylene glycol (EG) based stable nanofluids, characterized by energy-dispersive X-ray, X-ray dispersion, Fourier transform infrared spectroscopy, scanning electron microscopy, and zeta potential. Viscosity and density analysis were investigated by varying temperatures (25 to 50 °C), and wt% (0.01 to 0.25). For 0.25 wt% at 50 °C, density increased by 2.45%, and viscosity by 133.5%. The development of a prediction model by processing the variational parameters with machine learning and studying properties such as characterization, stability, and density of rGO-Fe3O4-TiO2 hybrid nanofluids has provided an unprecedented study in the literature. The nonlinear nature and volume of data generated by the subsequent experimental study were difficult to model using traditional analytical methods. As a result, for the creation of prognostic models, advanced machine learning techniques such as Boosted Regression Tree (BRT), Support Vector Machine (SVM), and Artificial Neural Networks (ANN) was applied. These prediction models' prognostic skills and uncertainty were assessed using statistical indices, Theil's statistics, and Taylor's diagram. The R-value for the BRT-based density (0.9989) and viscosity (0.9979) prediction models was higher than that of the ANN-based and SVM-based prediction models. In developed density models, Theil's U2 uncertainty was as low as 0.0689, 0.0775, and 0.0981 for BRT, ANN, and SVM, respectively. As a conclusion, it is stated that BRT, ANN, and SVM can accurately imitate the laboratory-based assessment of density and viscosity values of ternary hybrid nanofluids over a wide temperature and nanoparticle concentration ratio range. On the other hand, the BRT was marginally better than ANN but much better than SVM. The current study's findings are appropriate for applications needing long-term stability and improved heat transfer performance.

1. Introduction

Conventional heat transfer liquids such as water (H_2O), ethylene glycol (EG), and oil compared to solid particles show lower thermal conductivity, which is clear from the thermal properties [1,2]. Scholars and researchers have performed investigations to augment the thermophysical properties of traditional fluids [3,4], and enhance heat transfer using turbulators [5]. Choi [6], in 1995, coined a novel class of nanofluids as an enhanced alternative to improve thermal performance. Nanofluids are prepared by suspending nanoparticles such as metallic, carbides, ceramics, and non-metallic of size around or smaller than 100 nm in a base fluid [7,8]. The excellent thermal performance and less agglomeration of nanofluids are observed compared to conventional fluids [9,10]. The larger surface area of nanoparticles improves the nanofluids' thermal performance and enhances the suspension stability as well [11,12]. Several researchers reported higher thermal conductivity of traditional fluids with a minimum particle loading [13,14]. Although, the studies on rheological properties such as viscosity and density are significant parameters to reveal fluidic

* Corresponding author at: Department of Sustainable and Renewable Energy Engineering, University of Sharjah, Sharjah, P. O. Box 27272, United Arab Emirates.
E-mail addresses: zsaid@sharjah.ac.ae, zafar.said@uspcase.nust.edu.pk (Z. Said).

https://doi.org/10.1016/j.powtec.2022.117190
0032-5910/

performance. Many investigations have been studied on enhancing nanofluids' properties, but it is still not enough [15,16]. Further research is needed to analyze the concerns and progressions of various factors on nanofluids [17,18]. The nanofluids have been utilized in numerous applications such as electronics [19], solar energy [20–22], nuclear reactors [23,24], automotive industry [25,26], medical [27], minimum quality lubrication [28,29], and heating and cooling of buildings [30].

The thermophysical performance of hybrid nanofluids is determined by viscosity and ambient air impact due to heat transfer when stopped at the streamline flow. Further research is performed in this subject, and yet requires significant attention [31]. Sundar et al. [27] investigated the friction barrier and heat transmission performance of MWCNTs/Fe_3O_4 hybrid type nanofluid via a round tube experimentally and determined that a declining trend in viscosity was managed. Eshgarf et al. [32] observed the impact on the viscosity of temperature and volume concentration of water-ethylene/MWCNT-SiO_2 nanofluid and observed non-Newtonian behavior. The viscosity is reduced by increasing the temperature.

Literature signifies that graphene nanofluids can enhance thermal conductivity compared to other nanofluids because graphene nanoparticles show excellent thermal conductivity [33]. It is a promising material because of the high mechanical strength and excellent favorable thermophysical characteristics of graphene, making it a remarkable candidate for nanofluids [34]. Graphene can be easily synthesized as nanoparticles, and the procedure is moderately cost-efficient. Few alterations in the graphene characteristics have been demonstrated in literature because of different manufacturing techniques to fabricate single or multi-layer graphene, such as graphene oxide layer exfoliation and mechanical cleavage and chemical vapor growth, etc. [34,35]. Researchers examine graphene layers for increasing the heat transfer ability of H_2O-based fluids [36,37]. Chemical vapor deposition is an efficient method to accumulate perpendicular positioned graphene nanosheets [31] and weak packing graphene density [38]. Investigations have established enhanced heat transfer ability of single-layer graphene, which is more significant than CNT, due to the excellent stability and higher thermal conductivity, which is one of the main challenges among many, which must be analyzed precisely. The use of functionalization techniques such as acid treatment and amino function, better ultra-sonication, and solvent to prepare stable graphene-based nanofluids [39,40].

The rheological nature of nanofluids prepared from a diverse type of base fluids and nanoparticles has been assessed in the literature [41,42]. Graphene (*Gr*) has been the most frequently utilized nanoparticle material in nanofluids owing to superior thermal conductivity [43,44]. Yang et al. [45] investigated the impacts of temperature ranges (20 °C to 80 °C), and particle loading concentration ranges (0 to 5.2 wt%) on silicone's rheological oil-graphene nanofluid and observed non-Newtonian shear-thinning behavior. A study by Li et al. [46] also computed graphene nanofluid viscosity that was solvent-free and observed that with the rising temperature from 20 to 70 °C, a reduction in viscosity from 67.6 to 16.99 Pa.s was observed. Processes like mechanical exfoliation [34], SiC procedure [47], and bottom-up fabrication from definite organic precursors [48], certainly decrease the graphene use for different purposes due to limited scalability and production cost expenses.

The investigational data regarding the studies' hybrid nanofluids density is restricted compared to other thermophysical properties like viscosity and thermal conductivity [49]. Ho et al. [50] investigated the hybrid Al_2O_3/H_2O nanofluids density and MEPCM particles concerning different mass concentrations at 30 °C in comparison to theoretical data. Yarmand et al. [51], examined the functionalized GNP–Pt hybrid nanofluids density for different nanoparticles particle loading concentrations such as 0.02, 0.06, and 0.1 wt% and temperatures ranged from 20 °C - 40 °C and observed improvement in density with the rise in concentration and decreases when temperature increases, the enhancement in the density of 0.11% at a 0.1 wt% concentration at 40 °C. The increase in density is attributed to the boundary effects on the bulk fluid properties generated by the surface of the nanoparticles, as well as the interfaces surrounding the nanoparticles, which are typically negligible. S. Askari et al. [52] examined the effect of density concerning concentration for hybrid Graphene-Fe_3O_4 and Fe_3O_4 nanofluids at ambient temperature. It was noticed that fluids' density improves when the particle concentration is increased [53]. The increase in density is insignificant at higher nanoparticle concentrations. However, since graphene has a lower bulk density than Fe_3O_4, the density of hybrid Graphene Fe_3O_4 nanofluids is lower than that of Fe_3O_4 nanofluids. Nanoparticles have a higher density than the base fluid in both nanofluids. With no changes in volume, nanoparticles are positioned between the layers of the base fluid. They increase the mass of the system while maintaining the same volume, resulting in an increase in density.

The experimental results regarding the characteristics of ternary rGO-Fe_3O_4-TiO_2 hybrid nanofluids show non-linear tendencies when temperature and concentration ratios change. Furthermore, the massive amount of data produced through experimental research was difficult to model using traditional approaches. In a generalized scheme of model prediction, a relationship is established between control factors and response variables. The traditional analytical methods suffer from poor prognostics and coupling abilities. This problem becomes more prominent in the case of nonlinear data. Machine learning methods prove to be superior in problem-solving based employing probability distribution model and statistical analysis [54]. This broadens the application scope of machine learning approaches significantly. Model prediction methods based on artificial intelligence (AI) such as genetic algorithm (GA), artificial neural network (ANN) [55], least-square support vector machine (LSSVM), adaptive neuro-fuzzy inference system (ANFIS), response surface methodology (RSM) [56,57], gene expression programming (GEP), various swarm optimization methods, and so on are capable of handling large amounts of data to create an efficient prediction model [58–60]. AI, as a trustworthy algorithm, can consider a wide range of variables. ANN has been used by several studies to predict the thermo-physical characteristics of mono and binary hybrid nanofluids, such as thermal conductivity [61,62], specific heat [63], a viscosity [64,65], and so on. However, the use of AI-based approaches to forecasting thermophysical characteristics and stability of hybrid nanofluids is still in its early stages [66]. In addition, the application of AI-based intelligent approaches to model forecasts the vast dataset of viscosity and density over a variety of temperature and concentration ratios would aid in the reduction of lab-based investigations [67].

Following the above-mentioned compressive literature survey, it was observed that no research has been conducted to investigate the rheology and density of the ternary rGO-Fe_3O_4-TiO_2 hybrid nanofluids proposed in this work, which necessitates careful attention utilizing systematic and theoretical engineering techniques. In consonance with the studies carried out in recent years, a new research direction has emerged to eliminate the research gap to determine the thermal and hydraulic characteristics of nanocomposites. The conspicuous side of this study is that a novel research on ternary hybrid nanofluids using such wide-ranging and machine learning techniques has not yet been presented in the literature. Moreover, the comparative use of three different machine learning methods is a driving force in demonstrating the originality of a truly unique work. This work discusses the characterization, stability, density, and rheology of a rGO-Fe3O4-TiO2 ternary hybrid nanofluid for the first time. The nanocomposites were prepared using the sol-gel method, and their characterization was successful. The thermophysical properties of hybrid nanofluids, including rheological behavior and density, were then investigated at concentrations ranging from 0.01 to 0.25 mass% and temperatures ranging from 25 to 50 °C. The study's findings may be applied to various technical applications, including cutting fluids and low-quality lubricants.

Furthermore, improvements in nanofluid velocity and density may incur a penalty in the form of pressure loss, resulting in increased

pumping power; hence, viscosity and density may be decisive considerations when selecting nanofluids for applications. The proposed nanofluid examined in this work has excellent stability and might be utilized in a range of engineering applications (such as lubricants), as well as other biomedical engineering and energy storage applications. The density and viscosity density of rGO-Fe_3O_4-TiO_2 ternary hybrid nanofluids were model predicted using three different machine learning techniques. In a first-of-its-kind investigation, the current study attempts to go beyond tried-and-true ANN and assess modern ensemble Boosted Regression Trees and Support Vector Machines techniques.

2. Experimental

2.1. Materials

Titanium (IV) butoxide precursor is used to synthesize TiO_2 nanoparticles. Graphite powder (100 mesh, ≥75% min), H_2SO_4, HCl, H_3PO_4, ethylene glycol ($C_2H_6O_2$), $KMnO_4$, and hydrogen peroxide 30% (H_2O_2), where the extra chemicals employed in the nanocomposite production. All chemicals were used by not carrying out additional distillation, and all are obtained from Sigma Aldrich.

2.2. Preparation of ferric oxide (Fe_3O_4) and graphene oxide (GO)

Graphite raw powder was used while synthesizing GO by the modified Hummers method, which was employed in the future while preparing ternary nanocomposites [68,69]. $FeSO_4$ and $FeCl_3$ were thermally decomposed in ethylene glycol with sodium acetate (NaAc) and ethanolamine, causing Fe_3O_4 nanoparticles to be synthesized [70,71]. Then, both Fe_3O_4 and GO nanoparticles, at 60 °C, are dried, for about one day, and the powder forms were prepared for the sol-gel technique to manufacture ternary nanocomposite.

2.3. Preparation of ternary nanocomposites

While synthesizing ternary rGO-Fe_3O_4-TiO_2hybrid nanocomposites, the simple sol-gel method was utilized [72]. Each element was obtained at an equal weight ratio during the nanocomposite preparation. In a few words, while nanoparticles were synthesized, 0.65 g of GO was dispersed in ethanol (260 mL), whereas 0.65 g of Fe_3O_4 was dispersed in 260 mL of ethanol individually. The mixture in question was sonicated for one hour. After probe sonication, the two solutions were mixed, following which the addition of 65 mL of titanium (IV) butoxide was performed. Finally, the solution was put in a 200 mL Teflon-lined stainless-steel autoclave and kept under nitrogen purge for ten hours before being heated at 180 °C. Following the end of the reaction, a greyish precipitate was obtained, its washing 3 times with ethanol, and then water was carried out for the impurity removal. The nanocomposite drying was performed in a vacuum chamber at 60 °C for about ten hours.

2.4. Characterization

The ternary nanocomposites' surface morphology was evaluated under SEM (TESCAN MIRA3 XMU). Each sample was pressed into potassium bromide pellets and then employed to investigate the nanocomposite's functional groups using FTIR spectrophotometer (Bruker: Tensor II) with an interval between 4000 and 500 cm^{-1}. The structural considerations of the nanocomposites generated were investigated using XRD (Rigaku DMAX IIIC). To evaluate the stability of the produced nanofluids, zeta potential values were acquired using a (Malvern Instruments, UK) analyzer.

2.5. Rheological and density characterization

Ethylene-glycol and DI-water, which have well-known viscosity values at 25 °C, are employed as calibration fluids for viscosity measurements of a variety of fluids [65,66]. To validate the measurement method, the findings are compared to well-known viscosity values of DI-water and ethylene-glycol given in the literature. To ensure that the rGO-Fe_3O_4-TiO_2nanoparticles in ethylene glycol were well dispersed without initial agglomeration, an ultrasonic probe mixer (Sonics & Materials Inc., USA) was used at 750 W for one hour, was used for suspension agitation. In the suspensions, no dispersant agent was used. Using a cone-and-plate system, each rheological measurement was performed using a stress-controlled rheometer (Malvern Kinexus Pro, UK). The cone had a diameter of 50 mm and an angle of 2°. During measurement, the cone-plate space was set at 0.05 mm. Temperature-controlled measurements with a precision of ±0.1 °C were made using a Peltier plate assembly. The probing of flow curves for nanofluid viscosity based on shear rate and nanofluid viscosity depending on temperature was carried out using non-linear viscoelastic measurements. The experiments were carried out at shear rates ranging from 1 to 1000 s^{-1}. The current research examined ethylene glycol-based nanofluids' rheology by making non-linear viscoelastic measurements with changing concentration and temperature.

An Anton-Paar (model DMA 4100 M) digital density meter was utilized for the density measurement of nanofluids and ethylene glycol. The calibration of the digital density meter was performed as a temperature function utilizing deionized water and ethylene glycol at variable temperatures. The density was measured at 25 to 50 °C, at an interval of 5 °C. Every experimental density value represented an average of a minimum of 10 measurements. The density measurement's uncertainty was predicted as 0.02%. Thermophysio-chemical characteristics of ethyl glycol are presented in Table 1. Fig. 1 shows the prepared ternary nanocomposite photographs, EG base fluid, probe sonicator, density meter, and rheometer.

2.6. Prognostic modeling

The AI-based ANN was considered to model the density and viscosity of test hybrid nanofluid. Subsequently, two modern ensemble machine learning techniques viz., Boosted Regression Tree (BRT) and Gaussian Process Regression (GPR) were used to develop prediction models.

2.6.1. Artificial neural network

The density and viscosity of ternary type hybrid nanofluid used in the present investigation was model predicted using an ANN with a feed-forward backpropagation mechanism. The proposed structure of the neural network for density and viscosity is shown in Fig. 2(a) and (b). In the input layer of the neural network designed for the density model, two neurons denote two input parameters that impact the density of hybrid nanofluids. Temperature, and nanoparticle concentration wt% were chosen as input parameters. Temperature, shear rate, and nanoparticle concentration were the input parameters for the viscosity model. It shows the number of layers in the network, the kind of transfer function, the number of hidden layers, and the optimal number of neurons.

Generally, a neural network contains multiple neurons that, when combined, may perform any specified function to complete a job [73,74]. Enough training data must be supplied to improve performance. In the current study, 70% of the data was used to train the network, with the remaining 30% split between testing and validation of the model. The input layer (independent variables), hidden layer (neurons, bias –B, weight –W), and output layer (neurons, bias –B, weight –W) are the three layers that make up an ANN (expected response). A weighted input (W × 1), a transfer function, and an output are all present in each neuron. The neural neuron is activated by the

Table 1
Characteristics (physical and chemical) of ethylene glycol.

Ignition temperature	Saturation concentration (air)	Molar mass	Melting point	Density	Boiling point	pH	Vapor pressure
410 (°C)	0.15 (g/cm^3)	62.07 (g/mol)	−13 (°C)	1.11 (g/cm^3)	197.6 (°C)	6–7.5	0.053 (kPa)

weighted sum of inputs, which is subsequently passed via a transfer function to give a single output to the output layer. Tansig (tangent sigmoid) and purelin (linear) activation functions are widely used in the hidden layer and output layer. The network continues to run until a compelling level of assessment accuracy is achieved.

2.6.2. Boosted regression tree

Boosting can build an integrated model from several basic regression tree models to offer more robust estimates of the response. This technique differs from standard regression-based approaches, which only produce a single "best" model. The BRT method combines the key benefits of regression tree-based methods, such as the ability to model non-linear complex data, the ability to automatically detect interactions between explanatory variables. Also, the fact that trees are built with variables that are useful for prediction, making BRT implicitly species-based. The single models in the BRT are classification and regression trees that are iteratively fitted by randomly picking a subset from the training data set. Furthermore, the single tree-based regression models are improved using a boosting method, which improves regression accuracy and overcomes the shortcomings of decision tree outcomes. In general, the boosting technique is a strong forward and stage-wise procedure for increasing the accuracy of the final model by minimizing the predetermined loss function [75,76]. It is based on the building, integrating, and averaging of individual models in an iterative process. In this study, the missing function in the boosting approach was a minor square function. The learning rate (LR) parameter in the BRT model determines the contribution of each decision tree in the model's creation; the lower the number of LR [77].

The boosting technique develops the final model in a forward step, gradually adding trees to the model and re-weighting the data to strengthen the prior bad tree predictions. Outliers are separated into a node and have no influence on splitting; therefore, the technique is unaffected by monotonic changes of explanatory variables. The user determines the complexity of the decision tree (i.e., the total number of trees and nodes in a tree). The residual value is calculated at the end of each regression tree. This sequence moves through the model stage by stage rather than step by step, so old trees aren't altered, but model estimates are updated when new trees are added [78]. This process continues until the defined number of trees is reached or the residual has reached its optimum value, at which point improvements in model estimates are negligible. A learning rate further defines the contribution, or weight, of each tree to the model. Based on the results of the boosted regression trees, the model can then quantify the relative influence of each predictor variable on the response variable. A detailed description of BRT is available in the literature [79,80].

Fig. 1. Figures of rGO-Fe_3O_4-TiO_2 nanoparticles (a), EG (b), Sonics VCX-750 Probe Sonicator (c-d), Density meter: DMA 4100 M (e), Malvern Kinexus Pro, UK Stress Controlled Rheometer (f).

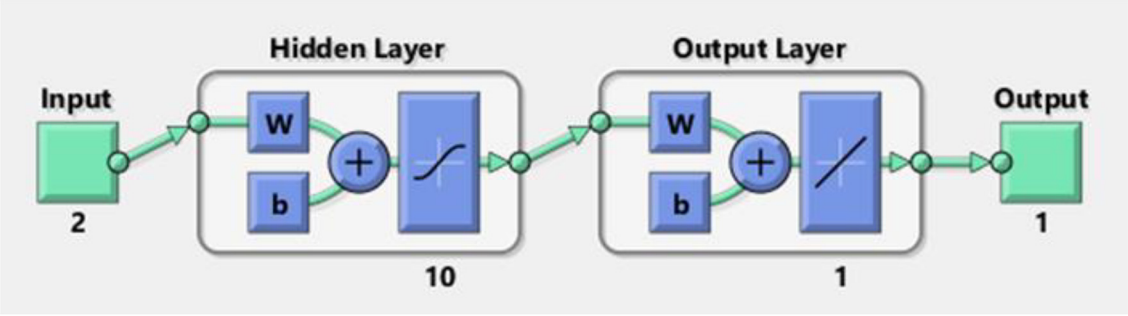

(a). Neural network structure for viscosity model.

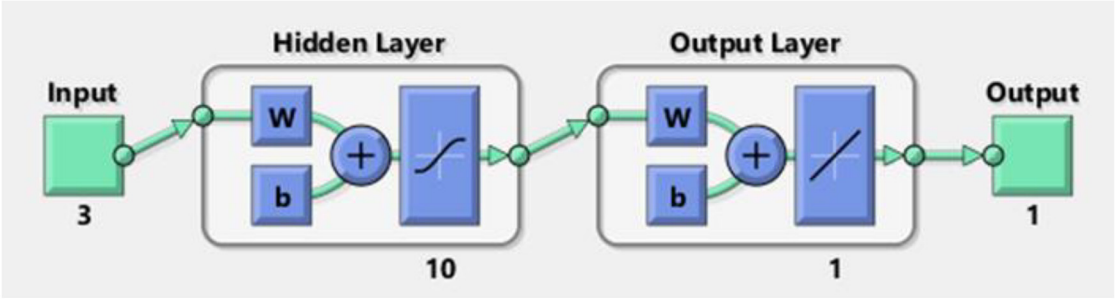

(b). Neural network structure for density model.

Fig. 2. (a). Neural network structure for viscosity model. (b). Neural network structure for density model.

2.6.3. Support vector machines

Cortes and Vapnik [81] were the first to suggest SVM, which was chosen as the modeling algorithm in this investigation. It is used for classification, regression, and outlier identification and belongs to the supervised learning category. The SVM design's goal is to examine a hyperplane in an N-dimensional feature space that accurately separates the different class points. Support vectors are feature points that are close to the hyperplane and have an influence on its position and arrangement. The margin between the classifier and the support vectors is optimized by support vectors. Hyperplanes serve as selection limits for labeling feature data. On either side of the hyperplane, data points may be associated with separate groups. The hyperplane's dimension is, however, determined by the number of feature points [82]. SVM is a relatively recent learning algorithm, and the main distinction between it and the other ML methods is that it decreases viable liability rather than decreasing classification error. The paradigm for this technique is to use hyperplanes to segregate feature points into the many classes to which they belong while maintaining the largest gap between classes. A nonlinear mapping moves feature points from primordial space to higher-dimensional feature space and searches for the best hyperplane [83].

Given a set of data, in which:

$$X = (x_1, x_2, x_3, \ldots\ldots, x_n), \tag{1}$$

also

$$Y = (y_1, y_2, y_3, \ldots\ldots, y_n) \tag{2}$$

x_n represents input, y_n is the forecast target variables. SVM aims to use the set of data to develop a function of regression $f(x)$capable of predicting target values from n numbers of inputs. The weight vector is denoted with w, b represents bias term, and non-linear model function is shown with $\psi(x)$, then the regression function can be shown as:

$$y = f(x) = w.\psi(x) + b \tag{3}$$

A detailed description of SVM for regression is presented by several researchers [84,85].

2.6.4. Model evaluation and uncertainty analysis

The modern machine learning-based models for viscosity and density were evaluated using established statistical measures. In the present study, Pearson's R, coefficient of determination (R^2), mean absolute percentage error (MAPE), root mean squared error (RMSE), Kling-Gupta efficiency (KGE) were applied to measure the prognostic ability of the model. Pearson's R denotes the strength of the correlation between measured and predicted values, while RMSE is a typical method of calculating a model's error in predicting quantitative data. The mean percentage error in prediction results is measured with MAPE. The KGE, which more evenly balances the three major components of the Nash-Sutcliffe efficiency (NSE) of predictive model's errors (i.e. ratio of variances, correlation, bias, or coefficients of variation), was also calculated in the present study [86]. The calculated values for these statistical measures are listed in Table 3. The following expressions (Eq. 4 to Eq.8) were used for statistical metrics:

$$R = \frac{\sum_{i=1}^{n}(x_i - \overline{x})(y_i - \overline{y})}{\sqrt{\sum_{i=1}^{n}(x_i - \overline{x})^2}\sqrt{\sum_{i=1}^{n}(y_i - \overline{y})^2}} \tag{4}$$

$$R^2 = 1 - \left(\frac{\sum_{i=1}^{n} (x_i - y_i)^2}{\sum_{i=1}^{n} (y_i)^2} \right) \quad (5)$$

$$RMSE = \sqrt{\sum_{i=1}^{n} \frac{(y_i - x_i)^2}{n}} \quad (6)$$

$$MAPE = \frac{1}{n} \sum_{i=1}^{n} \left| \frac{x_i - y_i}{x_i} \right| \times 100 \quad (7)$$

$$KGE = 1 - \sqrt{(\beta - 1)^2 + (\alpha - 1)^2 + (r - 1)^2} \quad (8)$$

where 'n' represents total elements, 'i' denotes term under consideration, 'x_i' denotes the actual value, 'yi' denotes predicted value, $\overline{x_i}$ is average of actual values, $\bar{y}$ is average of predicted values, 'β' denotes bias error, 'α' denotes error in flow variability, and correlation is shown with 'r'.

Thiel's statistics were used in the present study to estimate the uncertainty in the prognostic model developed for viscosity and density. Theil proposed two statistical measures for predictive models. The first one is, Theil's U1 which is used for the evaluation of prediction accuracy. However, Theil's U2 (also known as Theil's U) is a more popular statistical measure used to estimate the forecast quality of the predictive model. Theil's U2 is a collection of mean error and error differences between observed and expected values [87]. It provides a broad range of standardized measurements, with a lower value indicating better prediction quality. The expression used for the calculation of Theil's U2 is appended below as Eq. (9):

$$\lceil U_2 \rceil_{Theil} = \left[\frac{\sqrt{\sum_{i=1}^{n} (y_i - x_i)^2}}{\sqrt{\sum_{i=1}^{n} x_i^2}} \right] \quad (9)$$

3. Result and discussion

3.1. Characterization

The FTIR spectra were measured for ranges from 4000 to 500 cm^{-1} to examine the functional groups confined to the surface of nanocomposites. The ternary nanocomposites' FTIR spectra and whether there are various absorption peaks from the sample are shown in Table 2 and Fig. 3c. According to the mentioned FTIR, there has been excellent composting of rGO-Fe_3O_4-TiO_2 nanocomposites, demonstrated by every absorption group's view from every material utilized [88–90].

The synthesized nanocomposites' morphology was examined by a scanning electron microscope (SEM). The nanocomposite's SEM image, showing the platelet-like structure, is demonstrated in Fig. 3a.

Table 2
Determined frequencies of the FT-IR spectra of rGO-Fe_3O_4-TiO_2.

Assignment	FTIR peak of rGO-Fe_3O_4-TiO_2 (cm^{-1})
O−H	3430
CH_2	2918
C=O carbonyl stretching vibration and which specifies the GO deoxidization in the solvothermal process	1729
C=C aromatic rings	1564
C−O	1200
Ti−O	700
Fe−O	560

There is the anchoring of Fe_3O_4 and TiO_2 across the GO surface. The figure shows that TiO_2 and Fe_3O_4 nanoparticles are distributed across rGO sheets. Areas of white color are named high-density regions, which are determined as Fe_3O_4, whereas gray areas are called TiO_2, and the remaining flakes of dark gray color are identified as rGO.

EDX analysis was accomplished for the rGO-Fe_3O_4-TiO_2 ternary nanocomposites to establish the elemental composition (Fig. 3b). The results of EDX analysis of rGO-Fe_3O_4-TiO_2 samples are presented in Table inserted in Fig. 3b. The spectra of rGO-Fe_3O_4-TiO_2 showed the characteristic peaks of O, Fe, C, and Ti.

Fig. 4 presents XRD patterns of rGO-Fe_3O_4-TiO_2 ternary hybrid composites. During the formation of rGO-Fe_3O_4-TiO_2, at 25.5° a broad anatase peak of TiO_2 is observed, which overlaps the characteristic peak of rGO [91,92]. At $2\theta = 11.2°$ diffraction peak of GO is observed [69]. Once the reaction has taken place, this peak disappears, and a new peak at $2\theta = 26°$ develops, showing the characteristic of rGO. Therefore, it is noticed that GO was decreased exclusively to rGO. A large intensity is observed due to the intersection of two peaks: TiO_2 and rGO, shown in Fig. 4. Prominent six diffraction peaks indexed are examined at30.6°, 36°, 43.44°, 53.35°, 57.6°, and 63.1° to (220), (311), (400), (422), (511), and (440) planes of Fe_3O_4 (JCPDS 65–3107), respectively. Furthermore, it is capable of allocating TiO_2 peaks to the tetragonal anatase phase (JCPDS 21–1272) spotted at 63°, 53.9°,48°, 37.8°, and 63° to (204), (105), (200), (004), and (101), respectively. While handling the ternary composite phase, the anatase phase of Fe_3O_4 and TiO_2 is kept. While handling the ternary composite, the anatase phase of TiO_2 and Fe_3O_4 is maintained. The crystalline behavior of the composite was defined by the distinct sharp peak that formed in the XRD. Configuration of the composite is validated to assemble anatase TiO_2, Fe_3O_4, and rGO, based on the description presented above.

3.2. Stability, density, and viscosity of rGO-Fe_3O_4-TiO_2/EG nanofluid

The stability is also a major concern that impacts nanofluids characteristics for several applications, and it is essential to investigate and examine the parameters that affect nanofluids' stability. The zeta potential is the electric potential in the interfacial double layer versus a point in the bulk fluid at the sliding plane's location outside the boundary. It depicts the possibility for change between the dispersion medium and the stationary fluid film near the suspended particle. The Zeta potential characterization has been employed to classify the ternary nanofluids' stability as this is one of the simplest and most important techniques to demonstrate the dispersion performance of nanoparticles. The zeta potential is significant because it is related to the stability of colloidal dispersions. Nanofluids with high zeta potential values, positive or negative, are electrically stable, whereas nanofluids with lower zeta potential values agglomerate. Nanofluids with zeta potential values between 40 and 60 mV are regarded as more stable. In comparison, those with a zeta potential of more than 60 mV are considered to perform better in terms of stability [93]. In general, the nanofluid is referred to have poor stability when the zeta potential values are less than 30 mV [94]. Nanoparticles in suspension may create clusters by intensifying size, descending due to gravity [93]. The zeta potential of ternary hybrid nanofluids with ranging particle loading from 0.01 to 0.25 wt% was carried out. Among various categories of graphene, GO comprises epoxide, hydroxyl, carboxyl, and carbonyl functional groups. Such clusters show excellent stability when combined with the base fluid [95].

The results show enhancement in the suspension stability of ternary nanofluids as compared to the rGO nanofluids. The reason may be that Fe_3O_4 and TiO_2 nanoparticles are combined and support the rGO surface. This means evading the overlapping and assembling layers of graphene and presented by SEM images as shown in Fig. 3. Hybrid nanofluid at 0.01 wt% showed+63.45 mV value of zeta potential, as displayed in Fig. 5. The zeta potential values were more than

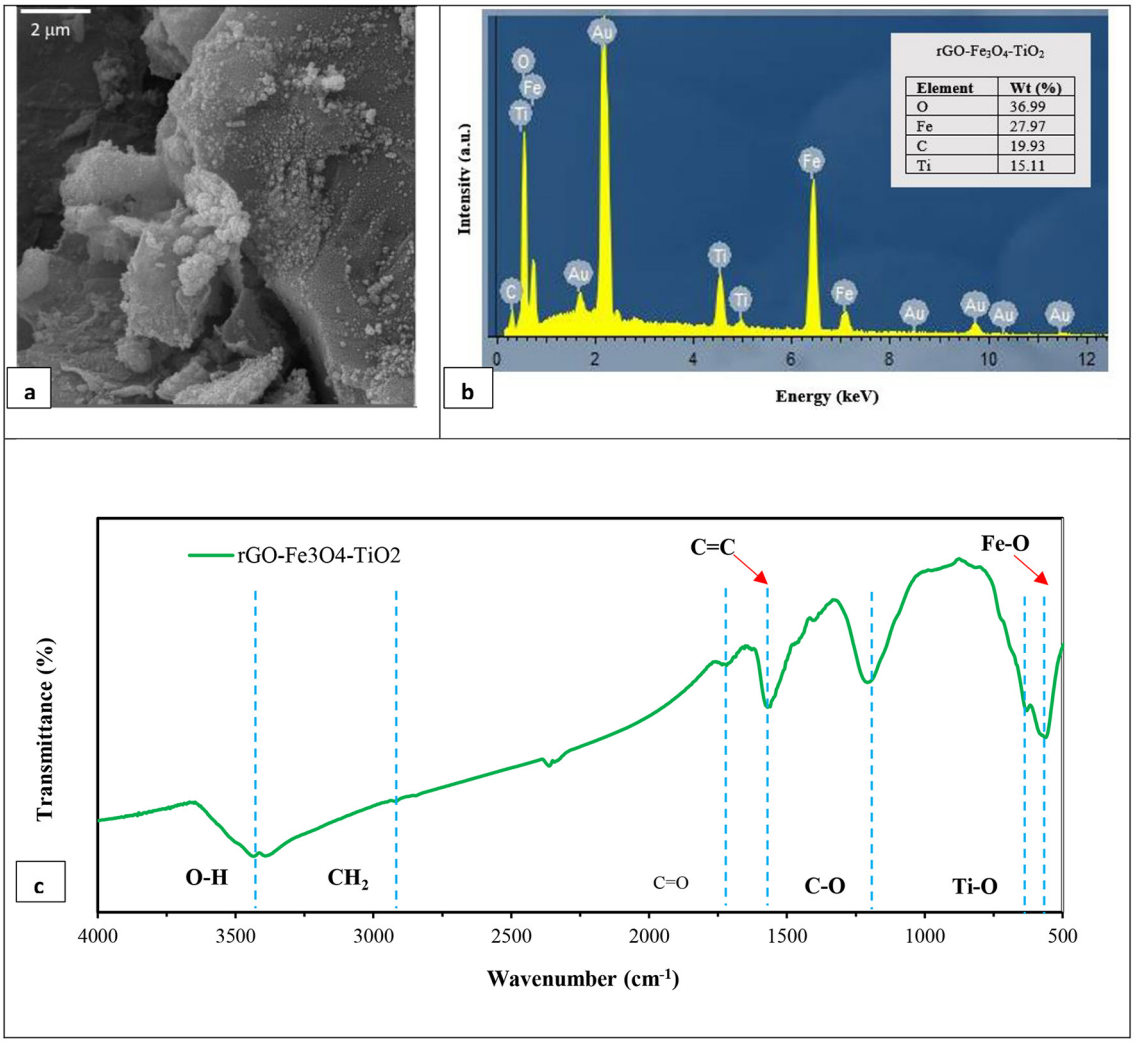

Fig. 3. a) SEM images of rGO-Fe_3O_4-TiO_2 b) Energy-dispersive X-ray spectroscopy (EDX) spectra, and c) FTIR spectra of rGO-Fe_3O_4-TiO_2 composites.

+52.43 mV for all samples obtained, which presents remarkable stability.

The density of ternary hybrid nanofluids is investigated with diverse weight fractions ranging from 0.01 wt% to 0.25 wt%. Density values of hybrid nanofluids at different temperatures are presented in Fig. 6 for different mass concentrations. Initially, to demonstrate the accuracy of

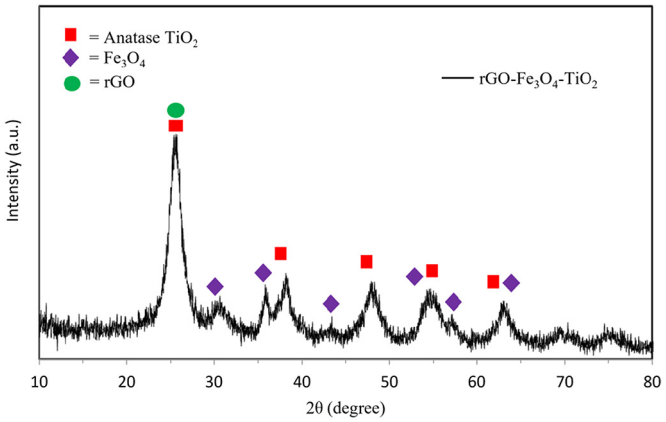

Fig. 4. Ternary hybrid nanocomposite with XRD patterns.

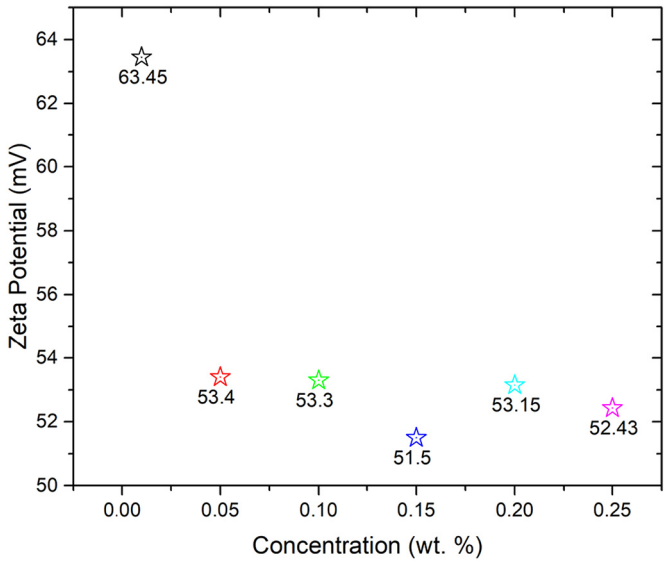

Fig. 5. Values of zeta potential for ternary hybrid nanofluid.

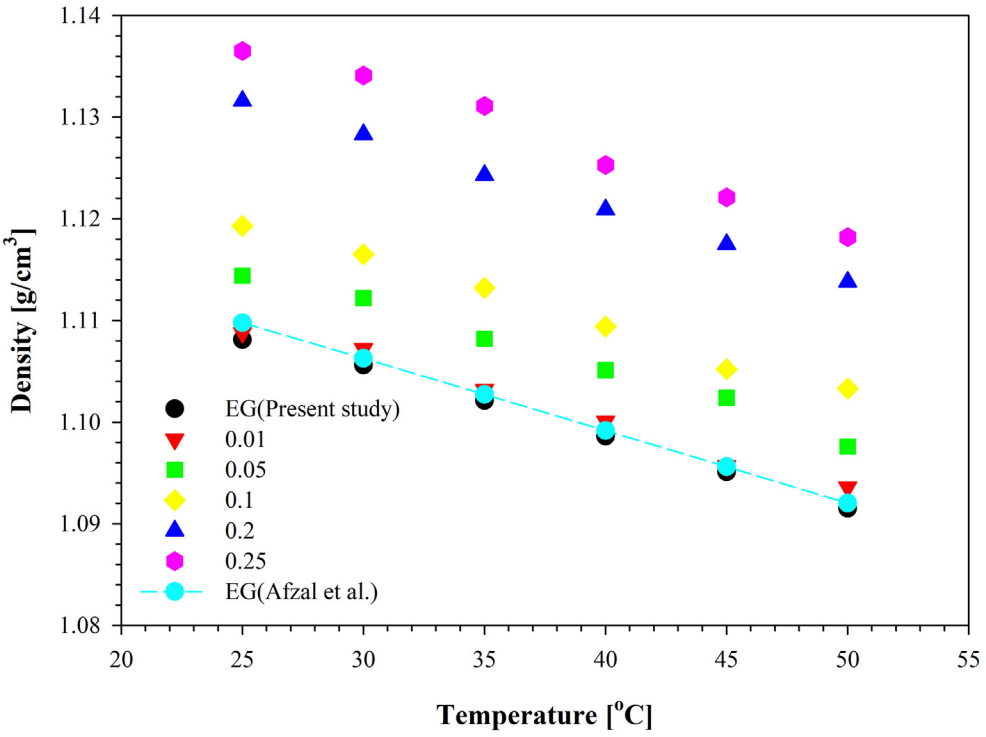

Fig. 6. Density versus temperature graph of rGO-Fe_3O_4-TiO_2/EG nanofluid at different mass fractions [96].

the experimental measurement analogy, pure ethylene glycol densities measured at varying temperatures were compared with Ref. [96] and as can be understood from this comparison, it is seen in Fig. 6 that the results of the present study and the referenced study are quite compatible. It is observed that at a low concentration of 0.01 wt% the density is almost similar to EG. As the mass concentration is increased, the density of rGO-Fe_3O_4-TiO_2/EG increases at different operating temperatures. However, when the temperature is raised, the density of nanofluids decreases. As density is a crucial parameter of hybrid nanofluids that significantly impacts the friction factor, Nusselt number, Reynolds number, and pressure loss, so in the present study, our attention is on computing the density of rGO-Fe_3O_4-TiO_2/EG nanofluids. The highest density was recorded at 0.25 wt% to be 1.13 (g/ml) at 25 °C. However, when the temperature was raised to 50 °C, the density dropped to 1.11 (g/ml). Aside from that, the density followed the base fluid's pattern. Similar trends as those in literature were obtained [61].

By applying a force that is regulated by the viscosity versus shear rate values, the viscosity of the nanofluid changes. The temperature and mass concentration of the rGO-Fe_3O_4-TiO_2 ternary nanocomposite generally impact the viscosity of the nanofluid. The viscosity of nanocomposite-based nanofluids decreases exponentially as the shear rate decreases [77]. The Newtonian and non-Newtonian behavior may be determined by plotting shear stress versus shear rates. A Newtonian fluid is defined as one that has a linear relationship between shear stress and shear rate. The Newtonian fluid is expressed as:

$$\tau = \mu.\gamma \tag{10}$$

where, shear rate and shear stress are given by γ and τ, respectively. The constant factor (μ) presented in the above expression is known as the fluid viscosity. For a Newtonian fluid, the value of viscosity is independent of the shear rate. Temperature affects the viscosity of nanofluids with Newtonian behavior. Non-Newtonian behavior is found when a linear relationship between shear stress and shear rate is not observed. It is necessary to describe a connection that is linked to the Newtonian fluid expression to model a fluid with non-Newtonian behavior [97,98]. The viscosity of different mass fractions (0.01 wt%, 0.05 wt%, 0.1 wt%, 0.2 wt%, and 0.25 wt%) of rGO-Fe_3O_4-TiO_2/EG ternary nanofluid was computed ranges from 25 °C to 50 °C. All measurements were repeated at various shear rates for each temperature and mass fraction for reliable findings.

The present experimental density ratio of rGO-Fe_3O_4-TiO_2/EG ternary nanofluid is compared with Oliveira et al. [99] data of ND-Ag/EG hybrid nanofluid and the comparison is made in Fig. 7. It is observed from the figure, the present data of rGO-Fe_3O_4-TiO_2/EG ternary nanofluid is showing higher values than the Oliveira et al. [99] data of ND-Ag/EG hybrid nanofluid. This is caused because of the use of ternary nanoparticles in the present study. The density of ternary nanoparticles is higher than that of the density of hybrid nanoparticles.

Shear rate viscosity for EG is presented for the range of 25 °C to 50 °C, shown in Fig. 8. A clear Newtonian behavior of pure EG for the studied temperature range and shear rate is observed. Moreover, with the rising temperature, a reduction in the viscosity of EG is observed.

The viscosity of the hybrid nanofluid increases as the mass concentration of nanoparticles increases at various temperatures, following a similar pattern. To be familiar with the rheological behavior such as non-Newtonian or Newtonian in the case of rGO-Fe_3O_4-TiO_2/EG nanofluids at several particle loading concentrations, the shear viscosity, which can be defined in terms of shear rate for the different mass concentration, ranges from 0.01 wt% to 0.25 wt% is displayed in Fig. 9. The linear trend between shear viscosity and the shear rate was observed, which signifies that rGO-Fe_3O_4-TiO_2/EG nanofluids show Newtonian behavior. Fig. 10 shows the variations in the shear viscosity versus the shear rate of rGO-Fe_3O_4-TiO_2/EG nanofluids at various temperatures with different particle loading concentrations. It is determined that raising the concentration increases the viscosity of nanofluids. It was also observed that the viscosity at lower temperatures is more significant than at high temperatures [100]. Fig. 11 shows the shear viscosity vs. shear rate trend at various

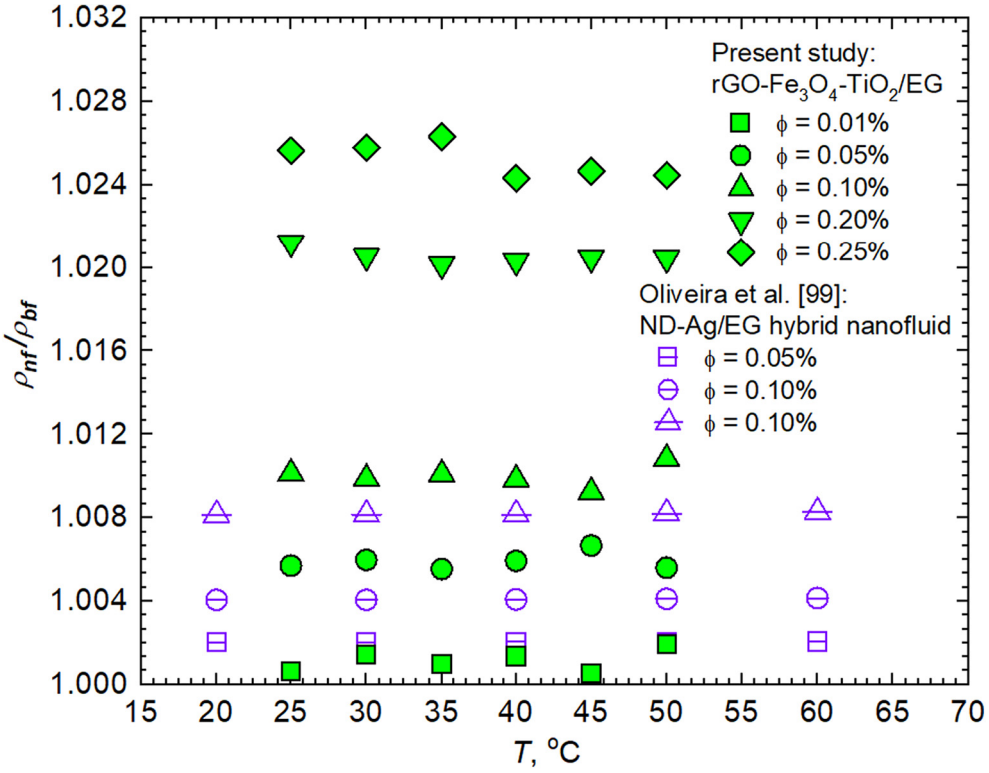

Fig. 7. Comparison of present experimental density of rGO-Fe_3O_4-TiO_2/EG ternary nanofluid with Oliveira et al. [99] data.

concentrations and temperatures. It can be observed that as the temperature rises, the viscosity reduces, but as the mass concentration rises, the viscosity rises to owe to the increased friction force between the fluid layers. Fig. 11 illustrates the shear viscosity as a function of temperature for varying concentrations from 0.01 to 0.25 wt% for GO-Fe_3O_4-TiO_2/EG and pure ethylene glycol viscosity values are validated with Ref. [101] for an accurate measurement. It is observed from the figure that viscosity decreases with rising temperature and becomes higher with higher particle loadings.

The results indicate the Newtonian behavior of rGO-Fe_3O_4-TiO_2/EG nanofluids. The molecules have entirely allied themselves at larger shear rates and achieved the highest shear classification because of the breaking molecules. This breaking down of molecules occurs because of weak particle—particle interfaces.

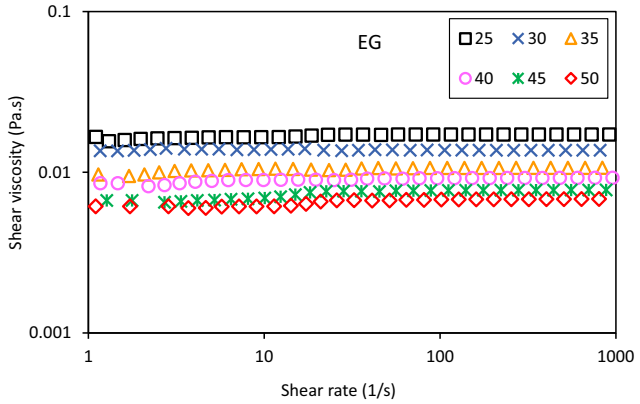

Fig. 8. Shear rate dependency of viscosity of ethylene glycol at different temperatures.

The friction between the fluid layers and viscosity is reduced as a result. Because of the cluster's growth in the fluid and internal viscous tension caused by adding more nanoparticles to the base fluid, the viscosity of various nanofluids gradually improves with increased mass concentration.

In the meantime, the viscosity declined by temperature rise because of the decrease in attractive molecular force. Furthermore, for all temperature ranges experimentally analyzed, viscosity is improved by increasing mass concentration. But, at high concentrations, the impact of temperature has intensely greater than at low concentrations. The agglomeration took place when the attractive forces of Brownian motion and Van der Waals of the nanoparticles were more substantial than repulsive forces sustained by DLVO theory [102]. The cumulative effects of Brownian motion, Van der Waals force, and electric charge repulsive force might be the cause of such viscosity variations. Conclusively, the higher viscosity is mainly due to the higher Van der Waals force, which could lead to aggregating the nanoparticles, therefore resulting in an increment in dynamic viscosity; however, with higher temperatures, the Van der Waals force becomes weaker, and the motion of the nanoparticles becomes intensified due to Brownian motion, which results in giving reduced viscosity at higher temperatures. With the increasing nanoparticles volume fraction, the viscosity enhanced, which is due to the larger slip resistances between the layers of the fluid, because of the addition of the nanoparticles [17].

The present study's obtained viscosity ratio results are compared to those reported in the literature by Kazemi et al. [103], Namburu et al. [104], and Sundar et al. [105], which are presented in Fig. 12. The results of the current study's viscosity ratio agree well with the data reported by Kazemi et al. as similar concentrations were studied. The viscosity ratio also showed a similar trend and data as those of Sundar et al. for lower concentrations of similar ones as the current study. The acquired results are in good conformity with the data provided in the literature, further validating our findings.

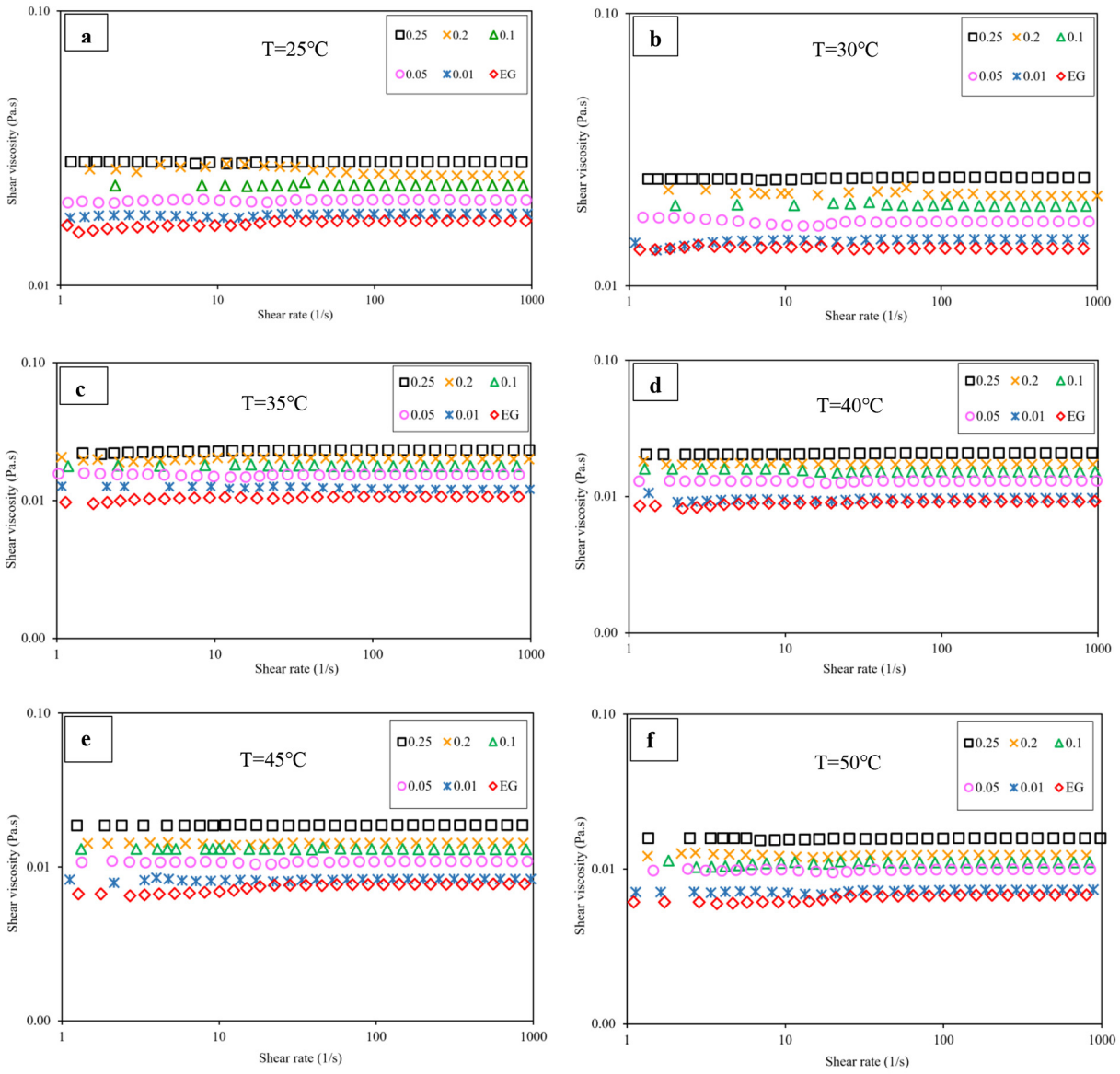

Fig. 9. Variations of the rGO-Fe_3O_4-TiO_2/EG viscosity versus the shear rate at different mass concentrations and temperatures (a) 25 °C, (b) 30 °C, (c) 35 °C, (d) 40 °C, (e) 45 °C, and (f) 50 °C.

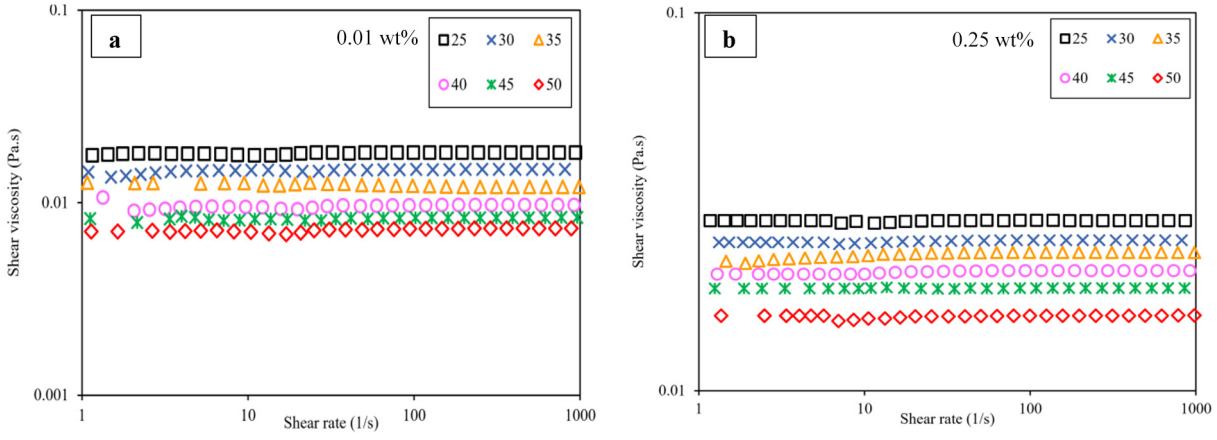

Fig. 10. Viscosity with respect to shear rate with changing temperature at 0.01 and 0.25 wt% of rGO-Fe_3O_4-TiO_2/EG.

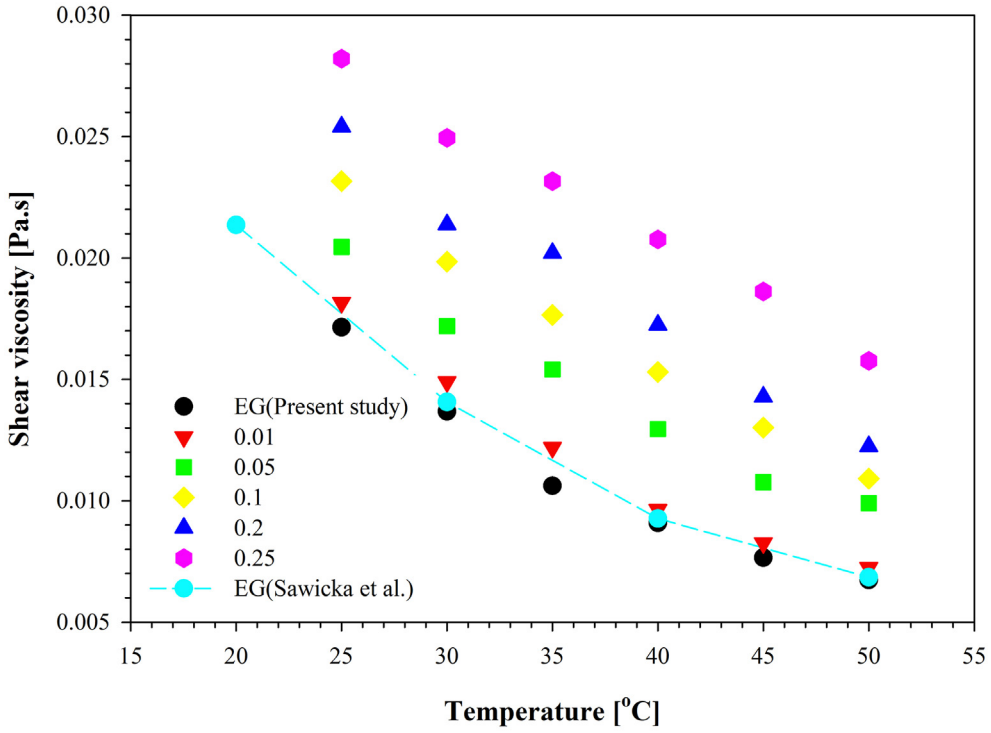

Fig. 11. Shear viscosity as a function of temperature for varying mass concentrations from 0.01 to 0.25 wt% rGO-Fe_3O_4-TiO_2/EG [101].

The obtained outcomes of viscosity are also compared with those reported by Sundar et al. [106] for hybrid (GO/Co_3O_4) nanoparticles suspended in EG as a base fluid, as shown in Fig. 13. Since similar particle loadings were investigated, this makes it ideal for the sake of comparison. It is observed from Fig. 12 that both the studies showed a similar trend and almost close values for the similar studied temperature range and particle loadings.

3.3. Modeling with ANN

In the present work, data were collected from the experimental characterization of rGO-Fe_3O_4-TiO_2 -EG ternary hybrid nanofluids was used for ANN-based modeling. The prognostic ANN model for density was prepared using temperature and nanoparticle concentration (wt%). The prediction model for viscosity was developed using

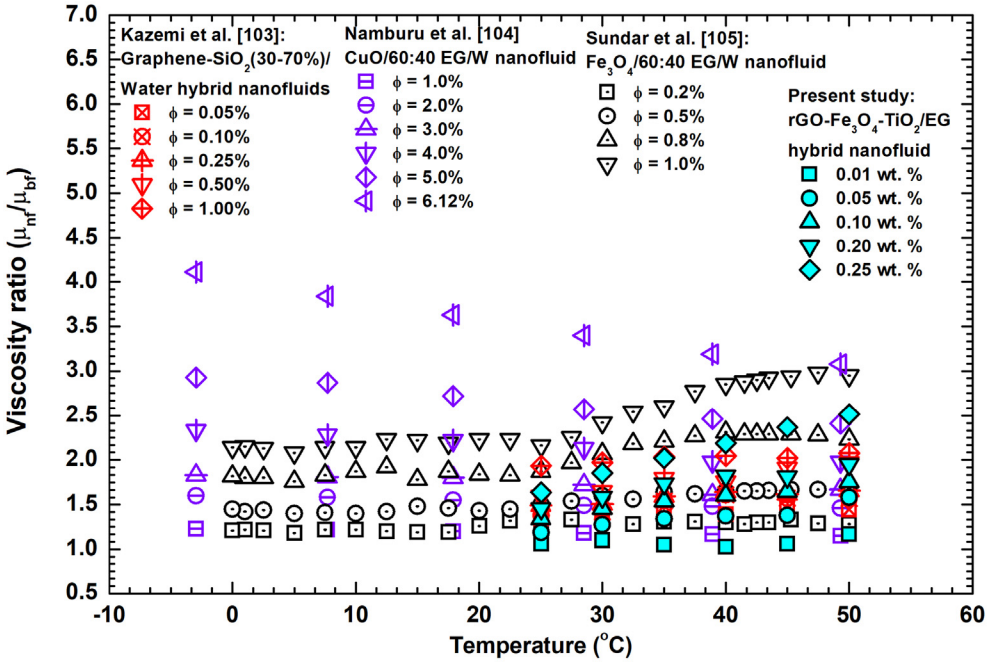

Fig. 12. Viscosity ratio comparison of current study with literature.

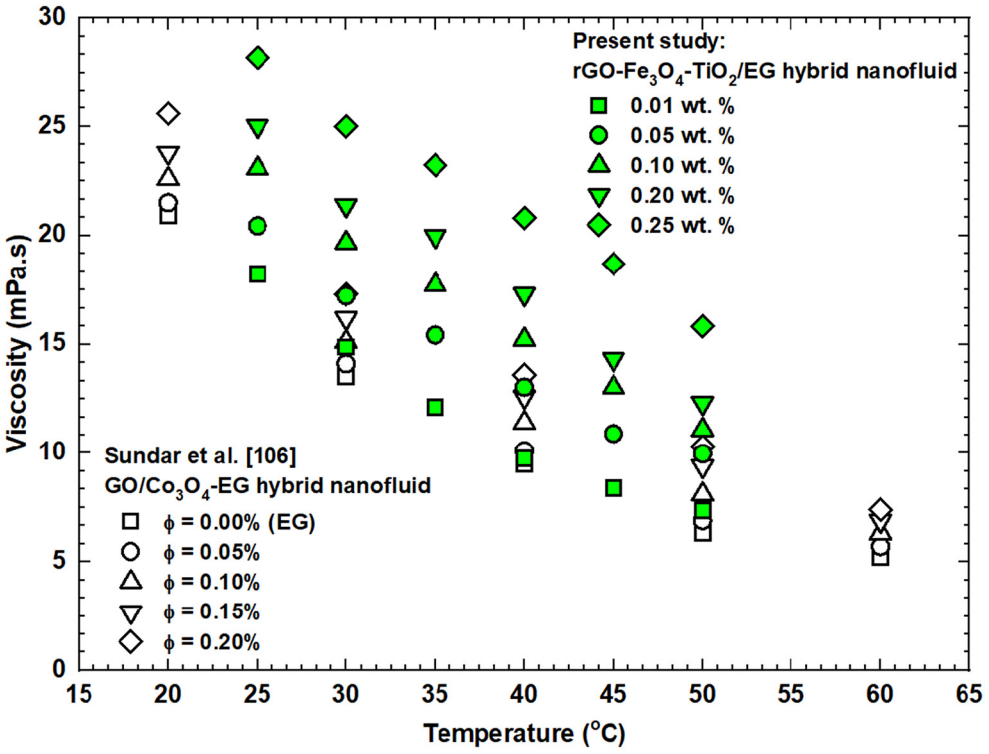

Fig. 13. Viscosity comparison of the current study with literature.

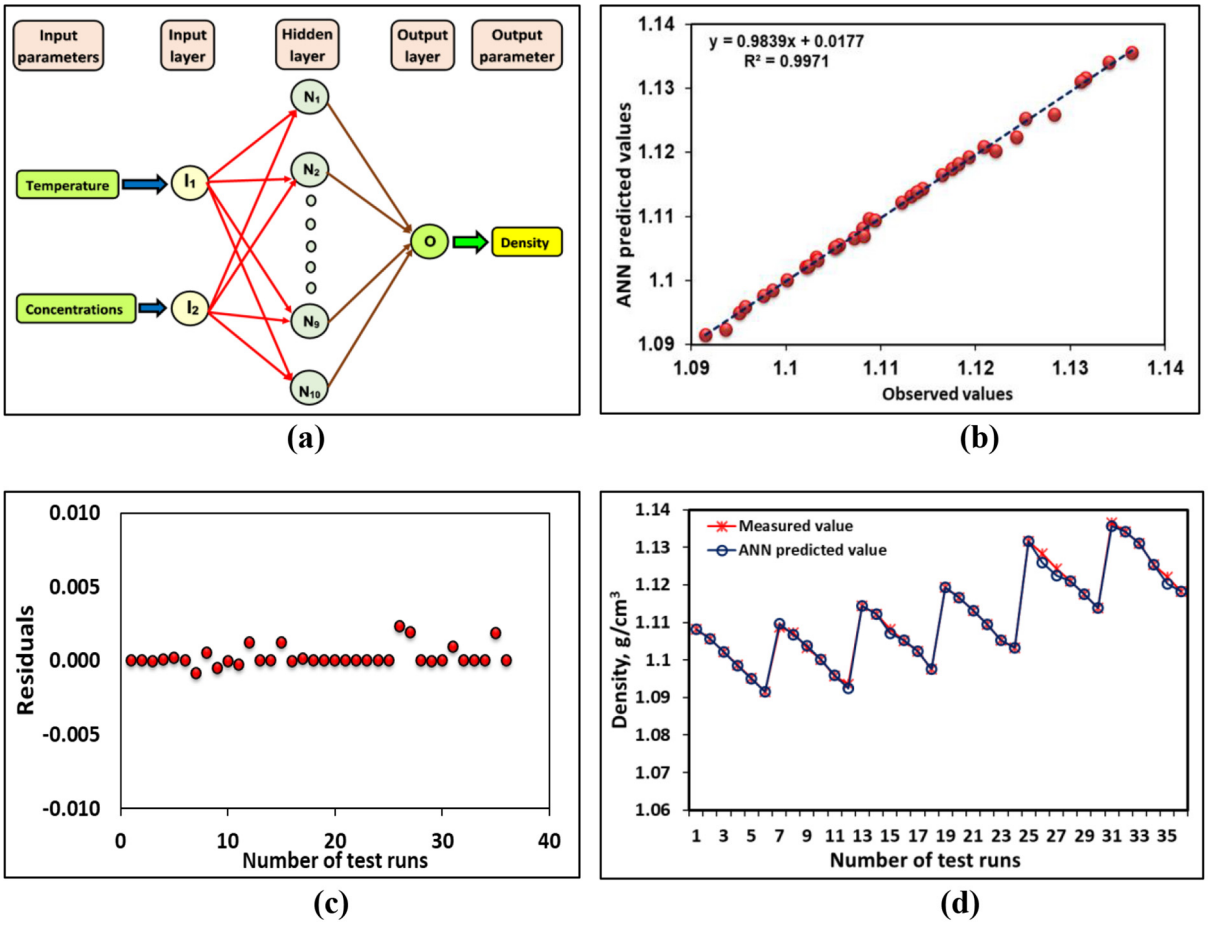

Fig. 14. ANN-based Density model (a) network architecture (b) regression graph (c) Model's residuals (d) Observed vs predicted values.

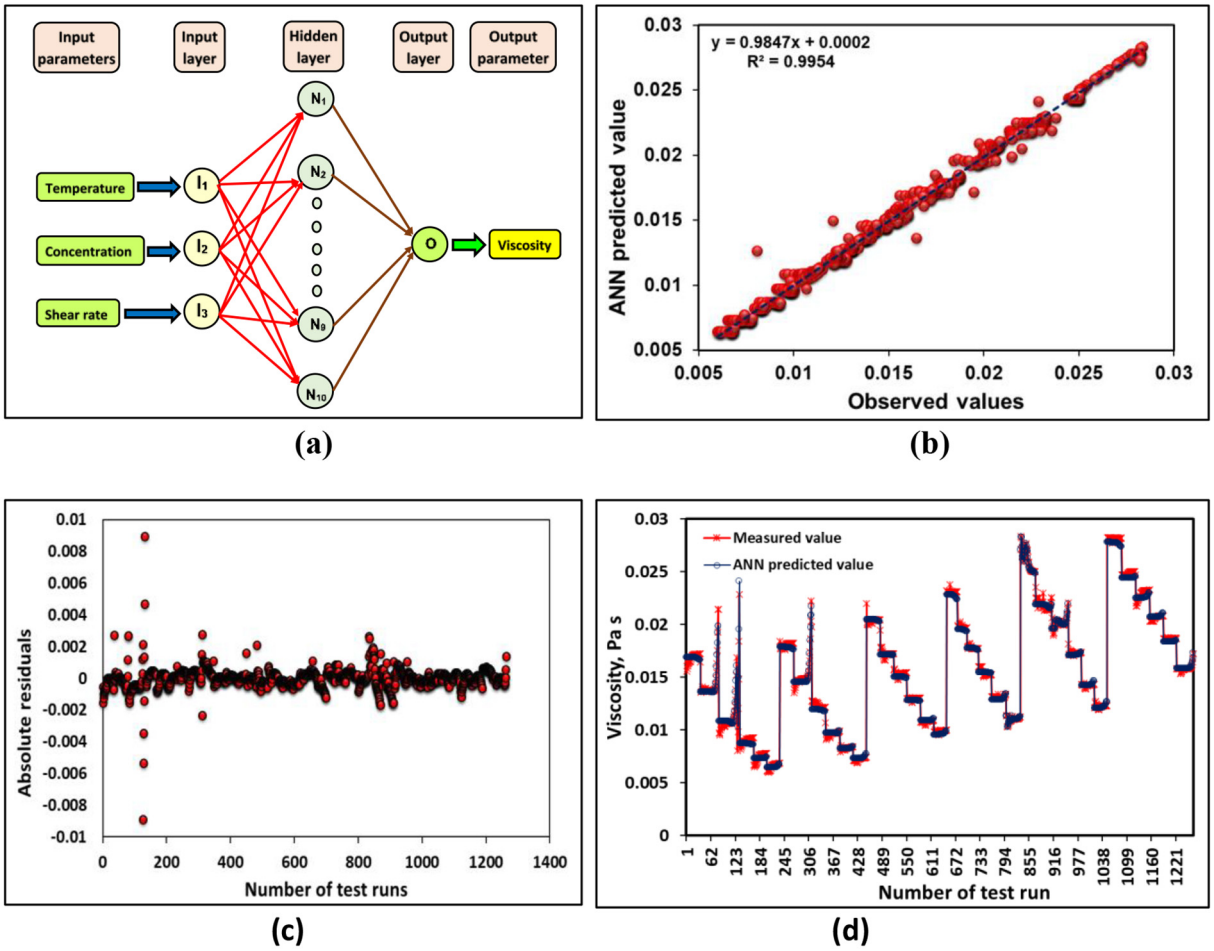

Fig. 15. ANN based viscosity model (a) network architecture (b) regression graph (c) Model's residuals (d) Observed vs predicted values.

temperature, nanoparticle concentration wt%, and shear rate. Two separate ANN model was developed for density and viscosity due to different input parameters.

3.3.1. Density model

The ANN-based predictive model for the density of ternary hybrid nanofluid (rGO-Fe_3O_4-TiO_2 -EG) was developed using the experimental data. The acquired data set was separated into three parts: 70% for training the network, 15% for testing and validation, and 5% for both. In the current ANN-based modeling, the commercial software MATLAB was utilized. The gradient descent technique (LEARNGDM) was utilized as the adaptive learning function to minimize the mean squared error (MSE) between the network output and the actual error rate. The hyperbolic tangent sigmoid transfer function (TANSIG) and linear transfer function (PURELIN) were utilized to generate a layer's output from its net input. The trial-and-error approach was employed during training to choose the number of neurons for the hidden layer. The ANN model architecture used for the density model is shown in Fig. 14(a).

Table 3
Statistical measures and uncertainty of ANN model.

Statistical measures						Uncertainty
Parameter	R	R^2	MAPE	RMSE	KGE	Theil's U2
Density	0.9985	0.9971	0.03%	0.0007	0.9858	0.0775
Viscosity	0.9972	0.9944	2.11%	0.00044	0.9971	0.129

For training, the network with the suggested ANN design (Fig. 14 (a)) with one input layer with two neurons, one hidden layer with ten neurons was used. The output layer with one neuron was used making it a multi-input and single output network. Once the ANN model was ready, it was used for density prediction on the entire input range of operating parameters. The regression line between observed and ANN model-based density values is illustrated in Fig. 13(b). An excellent 'R' (0.9985) and 'R^2' indicate an efficient prognostic model developed using ANN. Fig. 13(b) shows that almost all the data is split across the 45° line, indicating excellent compatibility between the test results and the ANN projected outcomes [107]. The residuals in the ANN-based model predicted values were low, as shown in Fig. 14(c). Barring a few data points, the error is low throughout the residual plot.

A comparative graph of measured viscosity and ANN-based model predicted viscosity for all the data points is illustrated in Fig. 14(d). Most of the ANN predicted and measured values of density almost replicate each other. The remarkable 'R' with low errors shows the excellent prognostic capability of ANN in modeling ternary hybrid nanofluid density in the present study.

3.3.2. Viscosity model

A data set containing 1264 elements, each for input and output parameters, was used for developing an ANN-based viscosity model. The obtained data set was divided into three parts, 70% for training the network, 15% each for testing and validation of the model. The gradient descent approach (LEARNGDM) was used as the adaptive learning function to reduce the mean squared error (MSE) between the network output and the actual error rate. The hyperbolic tangent sigmoid

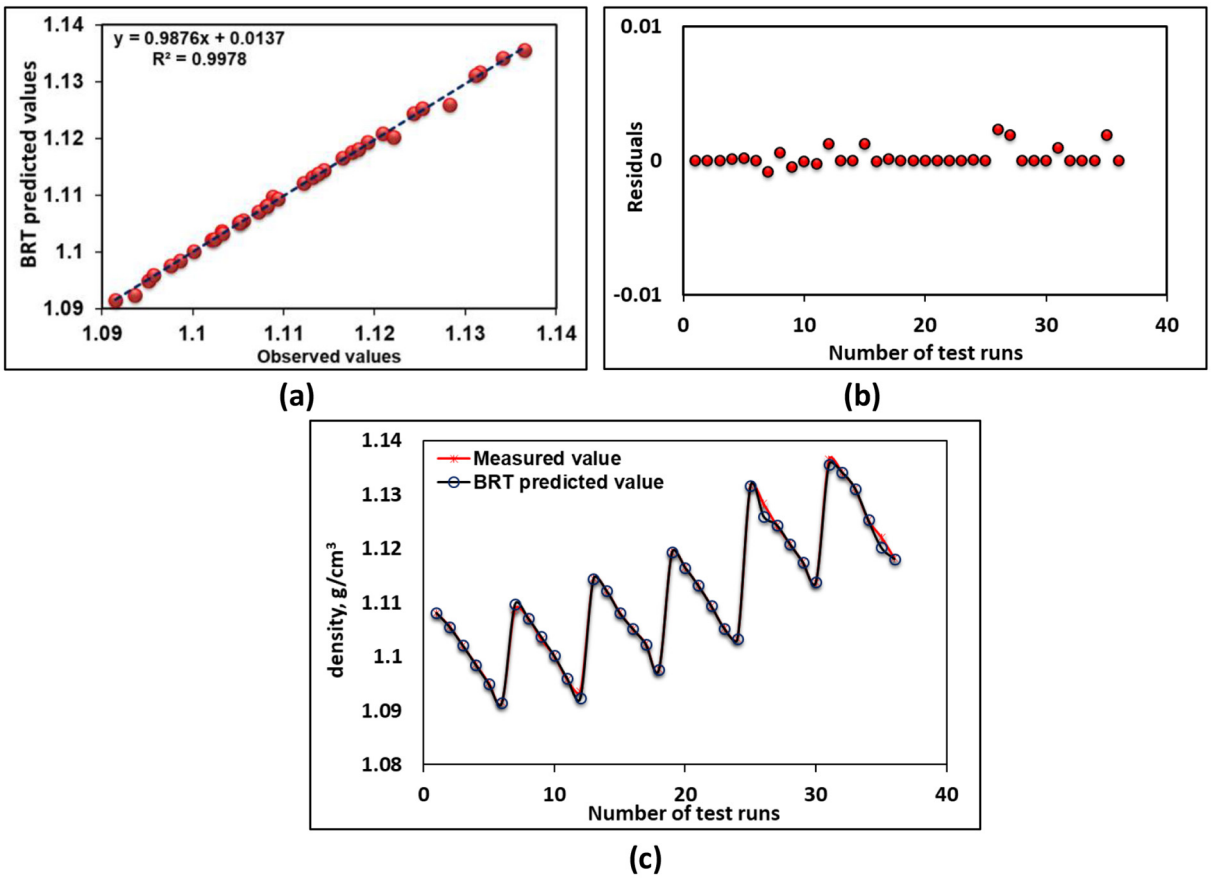

Fig. 16. BRT based density model (a) regression graph (b) Model's residuals (c) observed vs predicted values.

transfer function (TANSIG) and linear transfer function (PURELIN) were used to compute a layer's output from its net input. The trial-and-error method was used during training to select the number of neurons for the hidden layer. The training was started with 6 neurons, and the number of neurons was increased by 2 in the next training. A comparative analysis of this data indicated the suitability of 10 neurons as it resulted in the least mean squared error (MSE), among all results. Based on this analysis, the architecture of the multilayered perceptron ANN was prepared, as shown in Fig. 15(a). For training, testing, and validation, the created network with one input layer with three neurons, one hidden layer with ten neurons, and one output layer with one neuron was utilized [55].

The developed artificial neural network-based model was used to predict the viscosity for the entire range of input parameters. A comparative graph depicting the observed and model forecasted viscosity values are shown in Fig. 15(b). The linear trend line and coefficient of determination are also shown. An excellent 'R' value of 0.9972 with 'R^2' as 0.9954, both close to '1', establishes it as an efficient model. Almost all the data is split across the 45° line, indicating excellent compatibility between the test results and the ANN projected outcomes [108]. The errors in the ANN model were low, as illustrated in Fig. 15(c). A comparative graph of observed and ANN-based model predicted viscosity is illustrated in Fig. 15(d). It is observed that most of the experimentally measured and predicted values are close to each other, indicating a robust predictive model.

3.3.3. Statistical analysis of ANN models

The ANN-based prediction model was evaluated with various statistical indices and its predictive uncertainty was measured with Theil's statistics as mentioned in Section 2.6.4. The model's MAPE was 0.03% and 2.11% while RMSE was 0.0007 and 0.00041 for density and viscosity, respectively (Table 3). On the model efficiency front, the KGE was 0.9858 and 0.9971 for density and viscosity, individually. Thiel's U2 value depicting the uncertainty in the model was 0.0775 for the density model while it was 0.129 for the viscosity model. The low errors, low predictive uncertainty, and high KGE efficiency demonstrate the superior prognostic capability of ANN-based density and viscosity models.

3.4. Modeling with BRT

The modern ensemble machine learning BRT technique was used to develop a prediction model. The data from acquired from the characterization process of rGO-Fe_3O_4-TiO_2-EG ternary hybrid nanofluids was employed. Temperature and nanoparticle concentration was used to create a predictive BRT model for density (wt. percent). Temperature, nanoparticle concentration in weight percent, and shear rate were used to create a viscosity prediction model. Due to different input values, two distinct BRT models were created for density and viscosity.

3.4.1. Density model

The density model developed using the BRT technique was used to forecast the density of hybrid nanofluids at different temperatures and wt% concentration. A comparative analysis of observed density values during characterization and BRT model-based predicted values is illustrated in Fig. 16(a). The comparative graph also has a linear trend line, correlation equation, and R^2 value. The BRT-based density model is established as an efficient model with an outstanding 'R' value of 0.9989 and 'R^2' of 0.9978, both near to '1'. Almost all the data is divided over the 45° line, suggesting that the test results and the ANN's predicted outcomes are quite similar. As shown in Fig. 16(b) the ANN model's

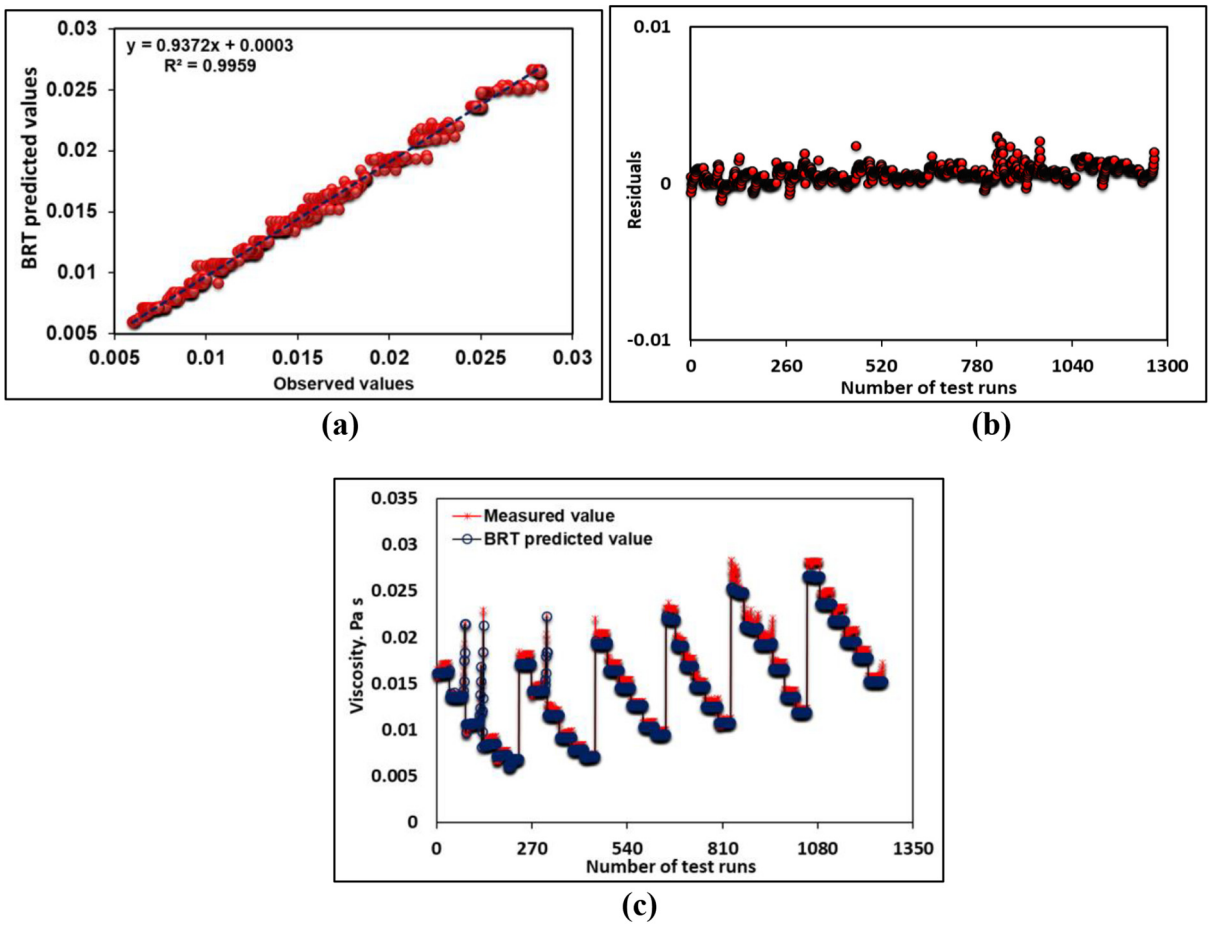

Fig. 17. BRT based viscosity model (a) regression graph (b) Model's residuals (c) observed vs predicted values.

errors were minimal. Fig. 16(c) shows a comparative graph of observed density and BRT-based model projected density for the entire range of test conditions [79]. Most of the experimentally measured and projected values were found to be near to each other, suggesting a reliable predictive model.

3.4.2. Viscosity model

The modern ensemble machine learning algorithm BRT was employed to develop the viscosity model. A data set collected from experimental characterization of rGO-Fe_3O_4-TiO_2-EG ternary hybrid nanofluids, containing 1264 elements, each for input and output parameters, was used for developing a BRT-based viscosity model. A comparative graph depicting the experimentally observed and BRT-based model predicted model is shown in Fig. 17(a). It was observed that all datapoints were close to the linear trendline with excellent 'R^2' as 0.9959, demonstrating a high degree of correlation between experimental and BRT-based model predicted values of viscosity [77]. A quadratic equation is also established to obtain a prediction for any input data. The robust quality of correlation is further established by a residual plot illustrated in Fig. 17(b).

Table 4
Statistical measures and uncertainty of BRT based model.

Statistical measures						Uncertainty
Parameter	R	R^2	MAPE	RMSE	KGE	Theil's U2
Density	0.9989	0.9978	0.004%	0.00059	0.9861	0.0689
Viscosity	0.9979	0.9959	2.03%	0.00035	0.9974	0.121

The BRT-based model was used to predict the viscosity of triple hybrid nanofluids used in this study. A comparative graph of experimental and forecasted viscosity values for all the data points is illustrated in Fig. 17(c). It is observed that both experimental and forecasted viscosity values are close to each other, demonstrating a robust prediction model [26].

3.4.3. Statistical analysis of BRT models

As indicated in Section 2.6.4, the BRT-based prediction model was evaluated using different statistical indices and its predicted uncertainty was assessed with Theil's statistics. The MAPE errors were 0.004% percent and 2.03%, respectively, while the RMSE was 0.00059 and 0.00035 for density and viscosity (Table 4). The KGE for density and viscosity, respectively, was 0.9861 and 0.9974 in terms of model efficiency. Thiel's U2 value, which represents model uncertainty, was 0.0689 for the density model and 0.121 for the viscosity model. The robust prognostic capacity of BRT-based density and viscosity models is demonstrated by the low errors, low prediction uncertainty, and high KGE efficiency [80].

3.5. Modeling with SVM

The MATLAB platform was used for the computational component of SVM-based modeling of density and viscosity of triple hybrid nanofluids used in this study. The Bayesian optimization function was used to optimize the SVM regression parameters. First, the SVM regression algorithm splits the experimental findings into training and testing datasets at random. Following that, the training dataset was normalized

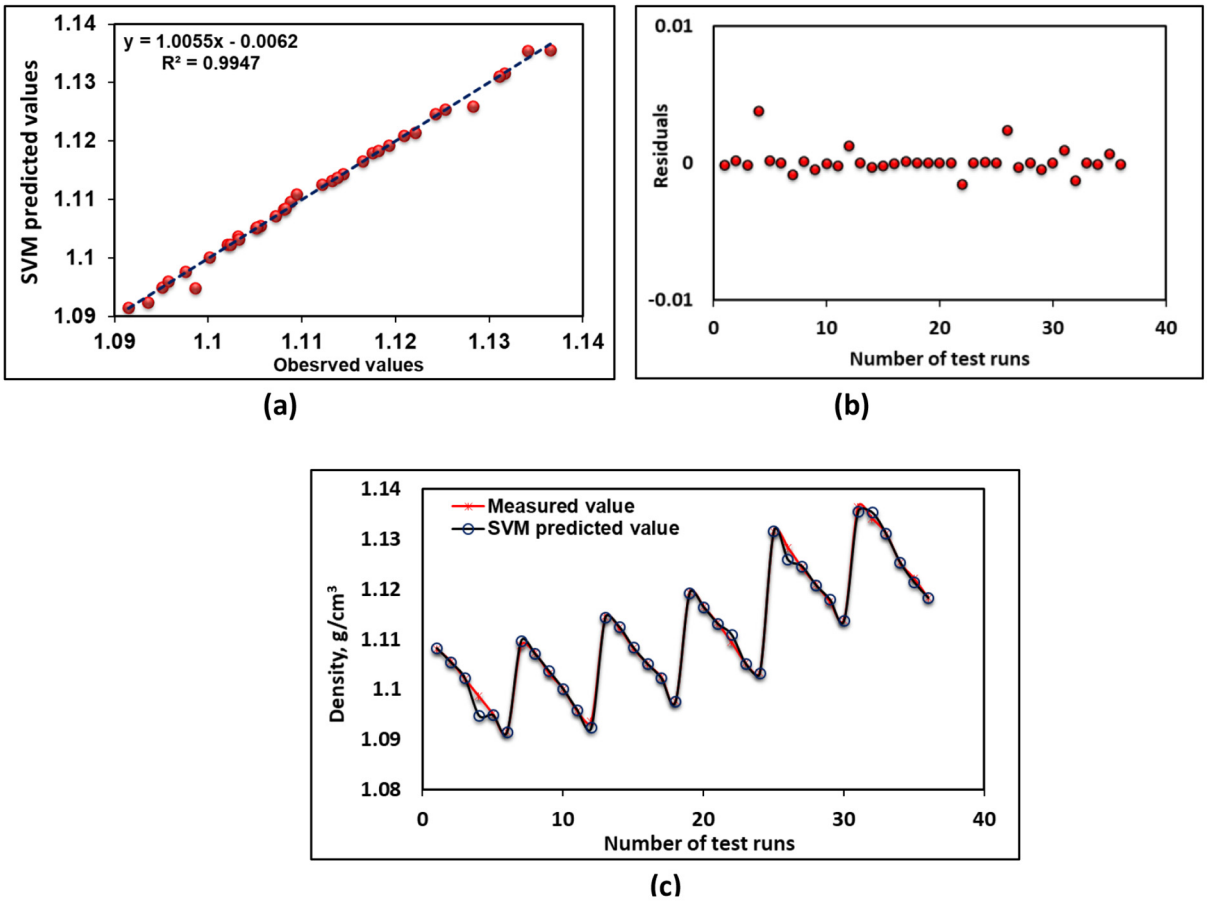

Fig. 18. SVM based density model (a) regression graph (b) Model's residuals (c) observed vs predicted values.

to ensure the model's computational efficiency. During the algorithm training, a 5-fold cross-validation process was used to ensure a robust model that could generalize well to a new dataset. The best SVM regression parameter values were determined by minimizing the training cross-validation error.

3.5.1. Density model

The density of hybrid nanofluids was predicted using a density model created using the SVM approach at various temperatures and weight percent concentrations. Fig. 18(a), shows a comparison between observed density values during characterization with predicted values based on the SVM model. A linear trend line, correlation equation, and R^2 value are also shown in the comparative graph. With an exceptional 'R' value of 0.9973 and 'R^2' of 0.9947, both close to '1', the SVM-based density model is proven as an efficient prediction model. The 45°-line divides almost all the data, implying that the test results and the SVM's projected outcomes are quite close. As shown in Fig. 18(b), a residual plot for the SVM-based prediction model further establishes the robust nature of association in observed and prediction data [83].

The observed and SVM model-predicted density of the triple hybrid nanofluids tested in this work over the entire range of input conditions is depicted in Fig. 18(c). Both experimental and projected density values are found to be near to one other, indicating a reliable prediction model over all the data points.

3.5.2. Viscosity model

SVM, a contemporary ensemble machine learning tool was used to develop a viscosity model. The prediction model was developed using data from experimental characterization of rGO-Fe_3O_4-TiO_2 -EG ternary hybrid nanofluids, which included 1264 components, each for input and output parameters. The developed model was used to predict the viscosity values over the entire range of input conditions. Fig. 19(a) shows a comparison graph of the observed and SVM-based model predicted viscosity values. All data points were found to be close to a linear trend line, with an outstanding 'R^2' of 0.9922, indicating a high degree of correlation between experimental and SVM-based model predicted viscosity values [84].

A quadratic equation is also established to produce a forecast for any input data. As shown in Fig. 19(b), a residual plot further establishes the strong nature of the association. The viscosity of the triple hybrid nanofluids utilized in this work was predicted using an SVM-based model over an entire range of input conditions. Fig. 19(c), shows a comparison graph of experimental and predicted viscosity values for all data points. Both experimental and projected viscosity values are found to be near to one other, indicating an efficient prediction model [85].

3.5.3. Statistical analysis of SVM model

The projected uncertainty of the SVM-based prediction model was examined using Theil's statistics and a variety of statistical indicators. The MAPE errors for density and viscosity were 0.04% and 2.95%, respectively, whereas the RMSE was 0.00088 and 0.00051 (Table 5). In terms of model efficiency, the KGE for density and viscosity were 0.9918 and 0.9728, respectively. The density model had a U2 value of 0.0981 and the viscosity model had a U2 value of 0.3686, which reflects model uncertainty. The low errors, low prediction uncertainty, and excellent KGE efficiency of SVM-based density and viscosity models indicate their strong prognostic potential [76,83].

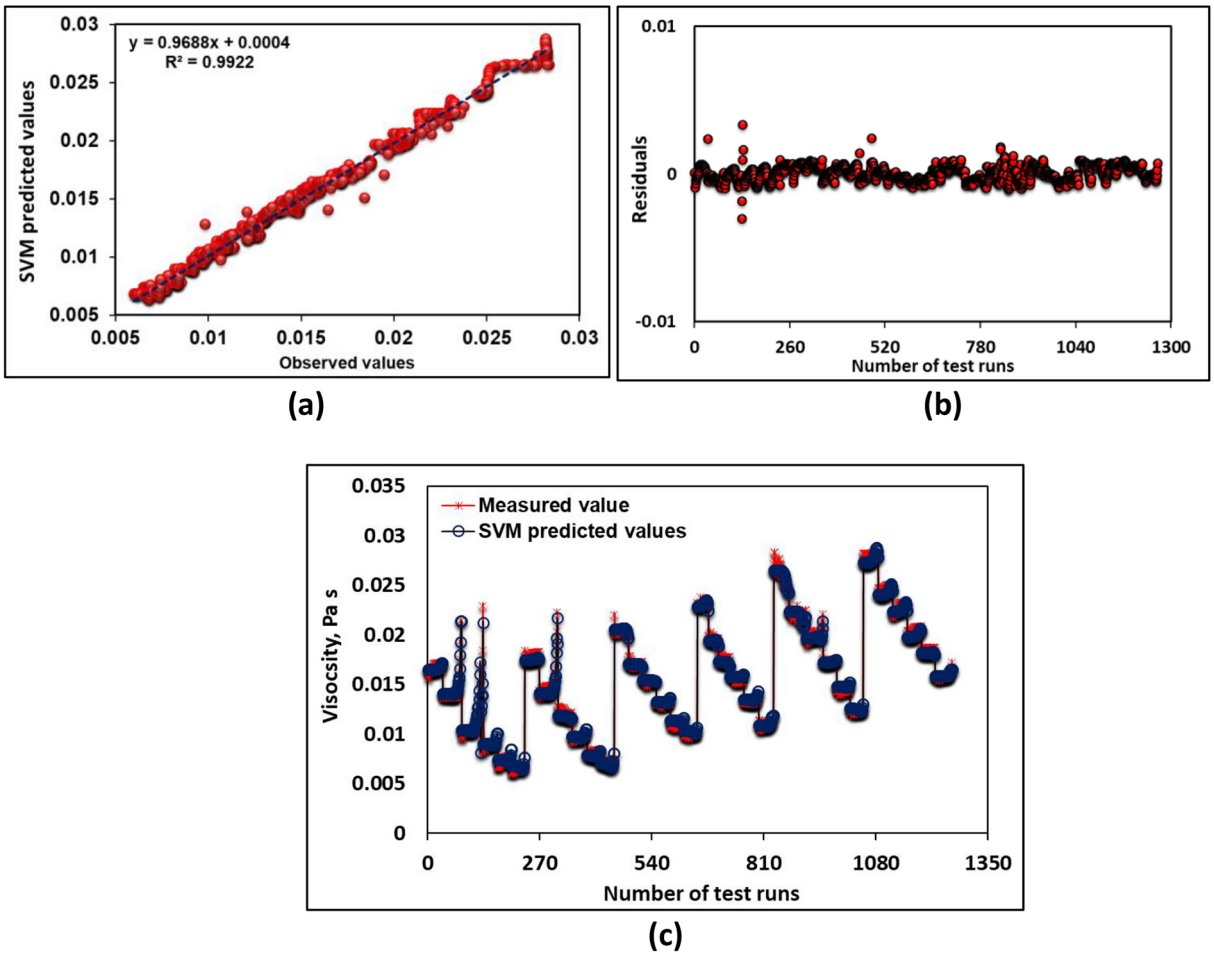

Fig. 19. SVM based viscosity model (a) regression graph (b) Model's residuals (c) observed vs predicted values.

3.6. Comparison of ANN, BRT, and SVM models

The preceding paragraphs indicate that all three machine learning approaches employed in this work were successful in developing extremely accurate prediction models. It does, however, provide a venue for comparative study of various techniques. For comparison evaluation, two alternative techniques were employed. First, the statistical evaluation, which included Theil' U2, was utilized, as shown in Tables 3, 4, and 6. Fig. 20 depicts the statistical indices utilized as bar graphs for all three-machine learning-based models. Taylor's diagram was then constructed in a single graph for simple visual comparative examination, as seen in Fig. 21. The bar graphs in Fig. 20 clearly illustrate that BRT is superior in terms of greater correlation coefficients and model errors. BRT outperforms both SVM and ANN in prediction efficiency (KGE) and model uncertainty (Theil's U2). Taylor's figure (Fig. 21) shows the same result: the BRT outperforms both SVM and ANN.

Table 5
Statistical measures and uncertainty of BRT based model.

Statistical measures						Uncertainty
Parameter	R	R^2	MAPE	RMSE	KGE	Theil's U2
Density	0.9973	0.9946	0.04%	0.00088	0.99181	0.0981
Viscosity	0.9960	0.9922	2.95%	0.0005	0.9728	0.3686

4. Conclusions

In the current study, a novel ternary nanocomposite is characterized by FTIR, SEM, EDX, and XRD. The stability of the prepared rGO-Fe_3O_4-TiO_2/EG ternary hybrid nanofluids was evaluated using the zeta potential approach. Later the nanofluids with excellent stability were tested experimentally for density, rheological behavior ranging from 25 °C to 50 °C, and volume concentration in a range of 0.01–0.25 wt%. Nanocomposites were fabricated through the sol-gel technique. The stability of all of the produced hybrid nanofluids was found to be above +52.04 mV, indicating good long-term stability. Lower zeta potential values resulted from the increase in concentration. All the prepared hybrid nanofluids showed increased density and viscosity with increased mass concentration and showed a decline in density and viscosity with higher temperatures. An increment of 0.06% at 25 °C for 0.01 wt %, and 0.19% at 50 °C for 0.01 wt%. the concentration of the rGO-Fe_3O_4-TiO_2 nanofluids was obtained in comparison with EG base fluid, and for 0.25 wt% at temperatures of 25 °C and 50 °C, an increment of 2.56% and 2.45% was observed, respectively. The increment in density observed is minimal.An increment of 8.2% at 25 °C for 0.01 wt%, and 8.2% at 50 °C for 0.01 wt%. the concentration of the rGO-Fe_3O_4-TiO_2nanofluids was obtained compared to EG base fluid, and for 0.25 wt% at temperatures of 25 °C and 50 °C, an increment of 64.5% and 133.5% was observed, respectively. The percentage increment in viscosity concerning other shear rates was similar for the entire range. Conclusively, the density and viscosity mainly rely on the suspended mass concentration of nanocomposites. Newtonian behavior for rheological behavior was observed for all the studied particle loadings and

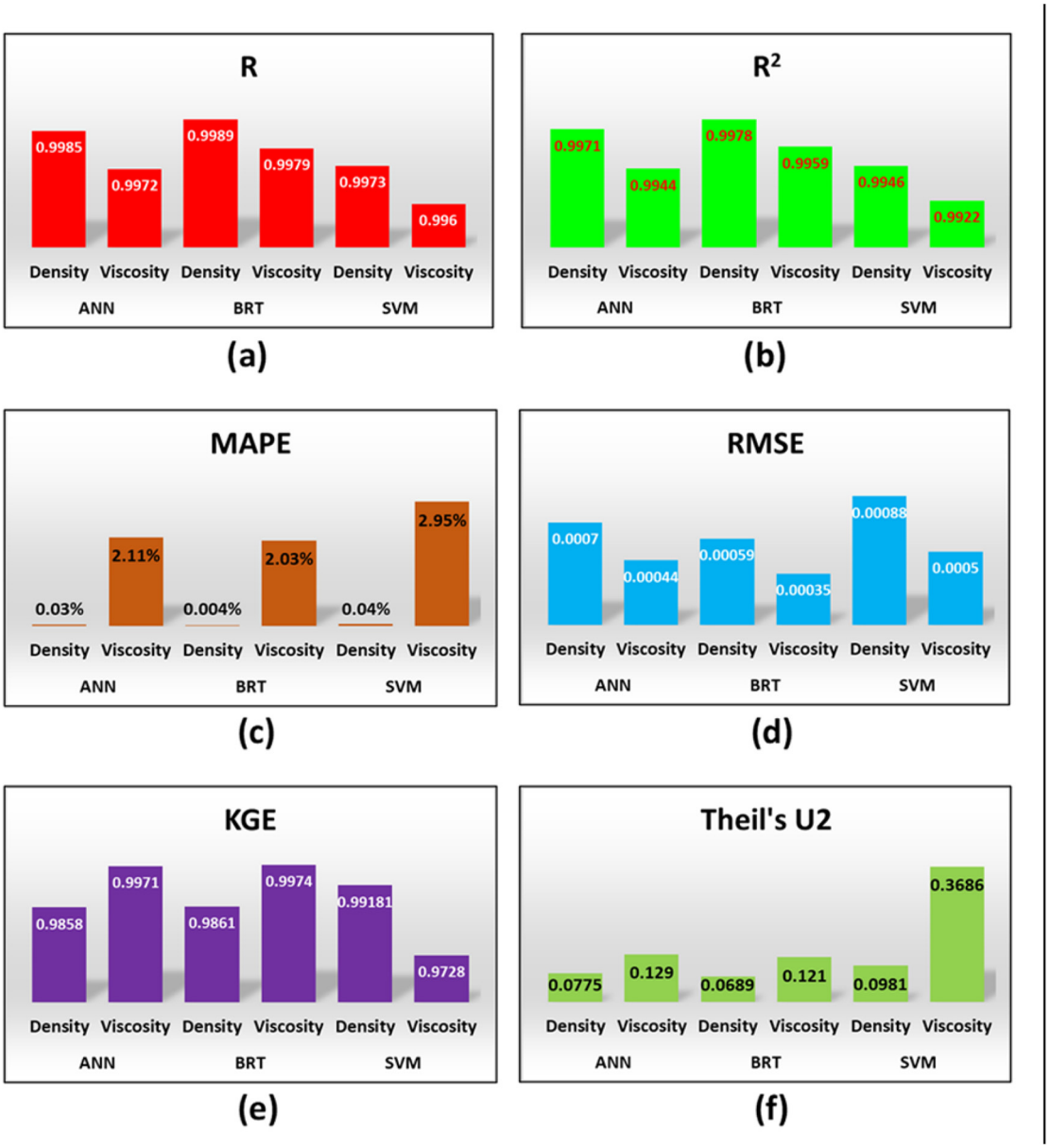

Fig. 20. Statistical indices of developed models.

temperatures. Two modern ensembles (BRT and SVM) and one neural network-based (ANN) machine learning technique were employed to model-predict the density and viscosity of ternary hybrid nanofluids. Using a statistical platform of error and performance measurements, the results of the generated models were compared to the real outcomes of the experimental research. The value of R for BRT-based density (0.9989) and viscosity (0.9979) model was superior to ANN-based and SVM-based prediction models. The value of R^2 (BRT > ANN > SVM) and KGE (BRT > ANN > SVM) demonstrates the superiority of BRT-based prognostic models. According to the error analysis, also the BRT reported lower MAPE and RMSE than both ANN and SVM. Theil's U2 uncertainty in developed density models was as low as 0.0689, 0.0775, and 0.0981 for BRT, ANN, and SVM, respectively. So, it is concluded that BRT, ANN, and SVM can accurately emulate the laboratory-based evaluation of density and viscosity values of ternary hybrid nanofluids for a diverse range of temperature and nanoparticles concentration ratios. The BRT, however, was marginally superior to ANN but more superior to SVM. The characterization of rGO-Fe_3O_4-TiO_2/EG ternary hybrid nanofluids, determination of properties such as stability and density, and then the development of a prediction model by using three different machine learning methods from the data obtained provides a unique study in the literature. In a way, a triggering study has been revealed that three different machine learning methods can be applied to similar studies, and it will encourage researchers in this context. In the future, we aim to further our studies by considering different Newtonian or non-Newtonian base fluids with different nanocomposites. It is planned to make applications in different technical fields such as diversified dimensional tubes in the different heat and cooling, microchannel heat exchanger, refrigeration, and air conditioning systems with nanofluids whose characterization analyzes have been completed. The present study outcomes are suitable for applications requiring long-term stability and higher heat transfer performance. These results discussed the stability, density, and viscosity of fluids, which may be used to determine pumping power, pressure drop, and lubricants in a variety of applications. Therefore, making the currently investigated ternary hybrid

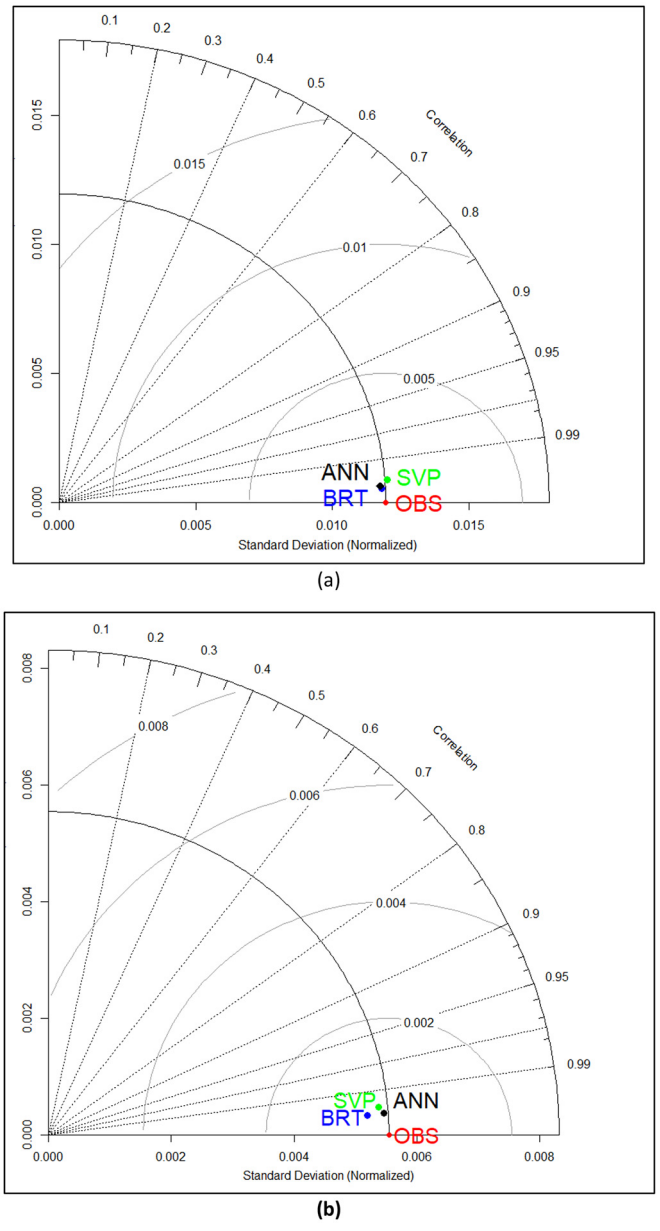

Fig. 21. Taylor's diagram (a) density model (b) viscosity model.

nanofluid a potential nanocomposite and nanofluid for various engineering and biomedical applications.

Nomenclature

AI	Artificial intelligence
ANFIS	Adaptive neuro fuzzy inference system
ANN	Artificial neural network
BRT	Boosted regression tree
CNT	Carbon nanotubes
DI	Deionized
EG	Ethylene glycol
FTIR	Fourier transform infrared spectroscopy
GEP	Gene expression programming
Gr	Graphene
KGE	Kling- Gupta efficiency
MAPE	Mean absolute percentage error
ML	Machine learning
MWCNT	Multi walled carbon nanotubes
NSE	Nash-Sutcliffe efficiency
RMSE	Root mean square error
RSM	Response surface methodology
SEM	Scanning electron microscopy
SVM	Support vector machines
XRD	X-ray dispersion
GNP	Graphene nanoplatelet
MEPCM	Micro-encapsulated phase change material
wt.	Particle mass fraction
W	Watt
T	Temperature, °C
mV	Milivolts

Greek symbols

γ	Shear rate, 1/s
τ	Shear stress, Pa
μ	Shear viscosity, Pa.s
c_p	Specific heat, J/Kg K
ρ	Density, kg/m^3

Declaration of Competing Interest

The authors declare that they have no known competing financial interests or personal relationships that could have appeared to influence the work reported in this paper.

Acknowledgments

The authors would like to thank Engr. Maham Aslam Sohail for her assistance. Dr. Zafar Said would like to thank the University of Sharjah, Projects #21020406162, for its financial support.

References

[1] A.A. Hachicha, et al., On the thermal and thermodynamic analysis of parabolic trough collector technology using industrial-grade MWCNT based nanofluid, Renew. Energy 161 (2020) 1303–1317.
[2] Z. Said, et al., Optimizing density, dynamic viscosity, thermal conductivity and specific heat of a hybrid nanofluid obtained experimentally via ANFIS-based model and modern optimization, J. Mol. Liq. (2020) 114287.
[3] M. Sheikholeslami, et al., Modification for helical turbulator to augment heat transfer behavior of nanomaterial via numerical approach, Appl. Therm. Eng. (2020) 115935.
[4] M. Sheikholeslami, S.A. Farshad, Investigation of solar collector system with turbulator considering hybrid nanoparticles, Renew. Energy 171 (2021) 1128–1158.
[5] M. Sheikholeslami, et al., Impact of new multiple twisted tapes on treatment of solar heat exchanger, Eur. Phys. J. Plus 137 (1) (2022) 86.
[6] S. Lee, et al., Measuring Thermal Conductivity of Fluids Containing Oxide Nanoparticles, 1999.
[7] R. Kiruba, et al., Stability and rheological properties of hybrid γ-Al2O3 nanofluids with cationic polyelectrolyte additives, Colloids Surf. A Physicochem. Eng. Asp. 555 (2018) 63–71.
[8] M. Sheikholeslami, S.A. Farshad, Numerical simulation of effect of non-uniform solar irradiation on nanofluid turbulent flow, Int. Commun. Heat Mass Transfer 129 (2021) 105648.
[9] M. Khattak, A. Mukhtar, S.K. Afaq, Application of nano-fluids as coolant in heat exchangers: a review, J. Adv. Rev. Sci. Res 22 (1) (2016) 1–11.
[10] I. Tlili, Impact of thermal conductivity on the thermophysical properties and rheological behavior of nanofluid and hybrid nanofluid, Math. Sci. (2021) 1–9.
[11] A. Aldabesh, et al., Thermal variable conductivity features in Buongiorno nanofluid model between parallel stretching disks: improving energy system efficiency, Case Stud. Therm. Eng. 23 (2021) 100820.
[12] S.U. Khan, et al., Bioconvection applications for double stratification 3-D flow of burgers nanofluid over a bidirectional stretched surface: enhancing energy system performance, Case Stud. Therm. Eng. 26 (2021) 101073.
[13] Z. Said, et al., Stability, thermophysical and electrical properties of synthesized carbon nanofiber and reduced-graphene oxide-based nanofluids and their hybrid along with fuzzy modeling approach, Powder Technol. 364 (2020) 795–809.
[14] Z. Said, A. Kamyar, R. Saidur, Experimental investigation on the stability and density of TiO2, Al2O3, SiO2 and TiSiO4, IOP Conference Series: Earth and Environmental Science, IOP Publishing, 2013.

[15] A.M. Ardekani, V. Kalantar, M. Heyhat, Experimental study on heat transfer enhancement of nanofluid flow through helical tubes, Adv. Powder Technol. 30 (9) (2019) 1815–1822.
[16] M. Gupta, V. Singh, Z. Said, Heat transfer analysis using zinc ferrite/water (hybrid) nanofluids in a circular tube: an experimental investigation and development of new correlations for thermophysical and heat transfer properties, Sustain. Energy Technol. Assess. 39 (2020) 100720.
[17] Z. Said, et al., Recent advances on nanofluids for low to medium temperature solar collectors: energy, exergy, economic analysis and environmental impact, Prog. Energy Combust. Sci. 84 (2021) 100898.
[18] N.K. Çakmak, H.H. Durmazuçar, K. Yapici, A numerical study of mixed convection heat transfer in a lid-driven cavity using Al2O3-water nanofluid, Int. J. Chem. Technol. 4 (1) (2020) 22–37.
[19] C.T. Nguyen, et al., Heat transfer enhancement using Al2O3–water nanofluid for an electronic liquid cooling system, Appl. Therm. Eng. 27 (8–9) (2007) 1501–1506.
[20] L.S. Sundar, et al., Energy, efficiency, economic impact, and heat transfer aspects of solar flat plate collector with Al2O3 nanofluids and wire coil with core rod inserts, Sustain. Energy Technol. Assess. 40 (2020) 100772.
[21] E. Bellos, C. Tzivanidis, Z. Said, A systematic parametric thermal analysis of nanofluid-based parabolic trough solar collectors, Sustain. Energy Technol. Assess. 39 (2020) 100714.
[22] Z. Said, et al., Heat transfer, entropy generation, economic and environmental analyses of linear Fresnel reflector using novel rGO-Co3O4 hybrid nanofluids, Renew. Energy 165 (2021) 420–437.
[23] J. Buongiorno, et al., Nanofluids for enhanced economics and safety of nuclear reactors: an evaluation of the potential features, issues, and research gaps, Nucl. Technol. 162 (1) (2008) 80–91.
[24] B.A. Khuwaileh, et al., On the performance of nanofluids in APR 1400 PLUS7 assembly: Neutronics, Ann. Nucl. Energy 144 (2020) 107508.
[25] H.M. Ali, et al., Heat transfer enhancement of car radiator using aqua based magnesium oxide nanofluids, Therm. Sci. 19 (6) (2015) 2039–2048.
[26] Z. Said, et al., Enhancing the performance of automotive radiators using nanofluids, Renew. Sust. Energ. Rev. 112 (2019) 183–194.
[27] H. Saleh, E. Alali, A. Ebaid, Medical applications for the flow of carbon-nanotubes suspended nanofluids in the presence of convective condition using Laplace transform, J. Assoc. Arab Univ. Basic Appl. Sci. 24 (1) (2017) 206–212.
[28] X. Wang, et al., Vegetable oil-based nanofluid minimum quantity lubrication turning: academic review and perspectives, J. Manuf. Process. 59 (2020) 76–97.
[29] Z. Said, et al., A comprehensive review on minimum quantity lubrication (MQL) in machining processes using nano-cutting fluids, Int. J. Adv. Manuf. Technol. 105 (5) (2019) 2057–2086.
[30] E. Firouzfar, et al., Energy saving in HVAC systems using nanofluid, Appl. Therm. Eng. 31 (8–9) (2011) 1543–1545.
[31] I. Mahbubul, R. Saidur, M. Amalina, Latest developments on the viscosity of nanofluids, Int. J. Heat Mass Transf. 55 (4) (2012) 874–885.
[32] H. Eshgarf, M. Afrand, An experimental study on rheological behavior of non-Newtonian hybrid nano-coolant for application in cooling and heating systems, Exp. Thermal Fluid Sci. 76 (2016) 221–227.
[33] Z. Said, et al., Recent advances on the fundamental physical phenomena behind stability, dynamic motion, thermophysical properties, heat transport, applications, and challenges of nanofluids, Phys. Rep. 946 (2022) 1–94, https://doi.org/10.1016/j.physrep.2021.07.002 In this issue.
[34] K.S. Novoselov, et al., Electric field effect in atomically thin carbon films, Science 306 (5696) (2004) 666–669.
[35] A. Kaniyoor, T.T. Baby, S. Ramaprabhu, Graphene synthesis via hydrogen induced low temperature exfoliation of graphite oxide, J. Mater. Chem. 20 (39) (2010) 8467–8469.
[36] M. Mehrali, et al., Investigation of thermal conductivity and rheological properties of nanofluids containing graphene nanoplatelets, Nanoscale Res. Lett. 9 (1) (2014) 15.
[37] W. Yu, et al., Significant thermal conductivity enhancement for nanofluids containing graphene nanosheets, Phys. Lett. A 375 (10) (2011) 1323–1328.
[38] Y. Yoon, et al., Vertical alignments of graphene sheets spatially and densely piled for fast ion diffusion in compact supercapacitors, ACS Nano 8 (5) (2014) 4580–4590.
[39] V. Sridhar, J.-H. Jeon, I.-K. Oh, Synthesis of graphene nano-sheets using eco-friendly chemicals and microwave radiation, Carbon 48 (10) (2010) 2953–2957.
[40] W. Zhang, W. He, X. Jing, Preparation of a stable graphene dispersion with high concentration by ultrasound, J. Phys. Chem. B 114 (32) (2010) 10368–10373.
[41] S.S. Murshed, P. Estellé, A state of the art review on viscosity of nanofluids, Renew. Sust. Energ. Rev. 76 (2017) 1134–1152.
[42] A. Hemmati-Sarapardeh, et al., On the evaluation of the viscosity of nanofluid systems: modeling and data assessment, Renew. Sust. Energ. Rev. 81 (2018) 313–329.
[43] O. Keklikcioglu, T. Dagdevir, V. Ozceyhan, Heat transfer and pressure drop investigation of graphene nanoplatelet-water and titanium dioxide-water nanofluids in a horizontal tube, Appl. Therm. Eng. 162 (2019) 114256.
[44] S. Alous, M. Kayfeci, A. Uysal, Experimental investigations of using MWCNTs and graphene nanoplatelets water-based nanofluids as coolants in PVT systems, Appl. Therm. Eng. 162 (2019) 114265.
[45] Y. Yang, et al., Characterization and convective heat transfer with nanofluids, ASME/JSME 2011 8th Thermal Engineering Joint Conference, American Society of Mechanical Engineers Digital Collection, 2011.
[46] P. Li, et al., Nanoscale ionic graphene material with liquid-like behavior in the absence of solvent, Appl. Surf. Sci. 314 (2014) 983–990.
[47] K.S. Novoselov, et al., A roadmap for graphene, Nature 490 (7419) (2012) 192–200.
[48] J.H. Warner, et al., Graphene: Fundamentals and Emergent Applications, Newnes, 2012.
[49] Z. Said, et al., Thermophysical properties of water, water and ethylene glycol mixture-based nanodiamond+ Fe3O4 hybrid nanofluids: an experimental assessment and application of data-driven approaches, J. Mol. Liq. (2021) 117944.
[50] C. Ho, et al., Preparation and properties of hybrid water-based suspension of Al2O3 nanoparticles and MEPCM particles as functional forced convection fluid, Int. Commun. Heat Mass Transfer 37 (5) (2010) 490–494.
[51] H. Yarmand, et al., Study of synthesis, stability and thermo-physical properties of graphene nanoplatelet/platinum hybrid nanofluid, Int. Commun. Heat Mass Transfer 77 (2016) 15–21.
[52] S. Askari, et al., Rheological and thermophysical properties of ultra-stable kerosene-based Fe3O4/graphene nanofluids for energy conservation, Energy Convers. Manag. 128 (2016) 134–144.
[53] H. Yarmand, et al., Experimental investigation of thermo-physical properties, convective heat transfer and pressure drop of functionalized graphene nanoplatelets aqueous nanofluid in a square heated pipe, Energy Convers. Manag. 114 (2016) 38–49.
[54] L. Shi, et al., Thermo-physical properties prediction of carbon-based magnetic nanofluids based on an artificial neural network, Renew. Sust. Energ. Rev. 149 (2021) 111341.
[55] Z. Said, et al., Synthesis, stability, thermophysical properties and AI approach for predictive modelling of Fe3O4 coated MWCNT hybrid nanofluids, J. Mol. Liq. (2021) 117291.
[56] P. Sharma, A.K. Sharma, Application of response surface methodology for optimization of fuel injection parameters of a dual fuel engine fuelled with producer gas-biodiesel blends, Energy Sources A (2021) 1–18.
[57] P. Sharma, Prediction-optimization of the effects of di-tert butyl peroxide-biodiesel blends on engine performance and emissions using multi-objective response surface methodology (MORSM), J. Energy Resour. Technol. (2021) 1–26.
[58] P. Sharma, Gene expression programming-based model prediction of performance and emission characteristics of a diesel engine fueled with linseed oil biodiesel/diesel blends: an artificial intelligence approach, Energy Sources A (2020) 1–15.
[59] Sharma, P., Artificial intelligence-based model prediction of biodiesel-fueled engine performance and emission characteristics: a comparative evaluation of gene expression programming and artificial neural network. Heat Transfer
[60] J. Wang, et al., Established prediction models of thermal conductivity of hybrid nanofluids based on artificial neural network (ANN) models in waste heat system, Int. Commun. Heat Mass Transfer 110 (2020) 104444.
[61] Z. Said, et al., Optimizing density, dynamic viscosity, thermal conductivity and specific heat of a hybrid nanofluid obtained experimentally via ANFIS-based model and modern optimization, J. Mol. Liq. 321 (2021) 114287.
[62] P.K. Kanti, et al., Experimental investigation on thermal conductivity of fly ash nanofluid and fly ash-Cu hybrid nanofluid: prediction and optimization via ANN and MGGP model, Part. Sci. Technol. (2021) 1–14.
[63] M. Jamei, et al., On the specific heat capacity estimation of metal oxide-based nanofluid for energy perspective–a comprehensive assessment of data analysis techniques, Int. Commun. Heat Mass Transfer 123 (2021) 105217.
[64] A.A. Alnaqi, J. Alsarraf, A.A. Al-Rashed, Using response surface methodology and artificial neural network to examine the rheological behavior of tungsten trioxide/ethylene glycol nanofluid under various sonication times, J. Mol. Liq. 337 (2021) 116022.
[65] S.U. Ilyas, et al., Rheological behavior of stabilized diamond-graphene nanoplatelets hybrid nanosuspensions in mineral oil, J. Mol. Liq. 328 (2021) 115509.
[66] Z. Said, et al., Thermophysical properties using ND/water nanofluids: an experimental study, ANFIS-based model and optimization, J. Mol. Liq. 330 (2021) 115659.
[67] T. Ma, et al., Recent trends on nanofluid heat transfer machine learning research applied to renewable energy, Renew. Sust. Energ. Rev. (2020) 110494.
[68] D.C. Marcano, et al., Improved synthesis of graphene oxide, ACS Nano 4 (8) (2010) 4806–4814.
[69] Q. Xiang, J. Yu, M. Jaroniec, Enhanced photocatalytic H 2-production activity of graphene-modified titania nanosheets, Nanoscale 3 (9) (2011) 3670–3678.
[70] D. Maity, J. Ding, J.-M. Xue, Synthesis of magnetite nanoparticles by thermal decomposition: time, temperature, surfactant and solvent effects, Funct. Mater. Lett. 1 (03) (2008) 189–193.
[71] A. Angermann, J. Töpfer, Synthesis of magnetite nanoparticles by thermal decomposition of ferrous oxalate dihydrate, J. Mater. Sci. 43 (15) (2008) 5123–5130.
[72] S. Banerjee, et al., Graphene oxide (rGO)-metal oxide (TiO2/Fe3O4) based nanocomposites for the removal of methylene blue, Appl. Surf. Sci. 439 (2018) 560–568.
[73] X. Yang, et al., Applying Artificial Neural Networks (ANNs) for prediction of the thermal characteristics of water/ethylene glycol-based mono, binary and ternary nanofluids containing MWCNTs, titania, and zinc oxide, Powder Technol. 388 (2021) 418–424.
[74] P. Sharma, A.K. Sharma, AI-based prognostic modeling and performance optimization of CI engine using biodiesel-diesel blends, Int. J. Renew. Energy Res. 11 (2) (2021) 701–708.
[75] A. Arabameri, B. Pradhan, L. Lombardo, Comparative assessment using boosted regression trees, binary logistic regression, frequency ratio and numerical risk factor for gully erosion susceptibility modelling, Catena 183 (2019) 104223.
[76] Y. Pan, et al., Estimation of real-driving emissions for buses fueled with liquefied natural gas based on gradient boosted regression trees, Sci. Total Environ. 660 (2019) 741–750.

[77] M. Jamei, et al., Specific heat capacity of molten salt-based nanofluids in solar thermal applications: a paradigm of two modern ensemble machine learning methods, J. Mol. Liq. 335 (2021) 116434.
[78] N. Ottman, et al., Soil exposure modifies the gut microbiota and supports immune tolerance in a mouse model, J. Allergy Clin. Immunol. 143 (3) (2019) 1198–1206 (e12).
[79] J.J. Vidal-Macua, et al., Assessing vegetation recovery in reclaimed opencast mines of the Teruel coalfield (Spain) using Landsat time series and boosted regression trees, Sci. Total Environ. 717 (2020), 137250.
[80] C. Persson, et al., Multi-site solar power forecasting using gradient boosted regression trees, Sol. Energy 150 (2017) 423–436.
[81] C. Cortes, WSupport-vector network, Mach. Learn. 20 (1995) 1–25.
[82] D.A. Pisner, D.M. Schnyer, Support vector machine, Machine Learning, Elsevier 2020, pp. 101–121.
[83] A. Asadi, et al., Feasibility of least-square support vector machine in predicting the effects of shear rate on the rheological properties and pumping power of MWCNT–MgO/oil hybrid nanofluid based on experimental data, J. Therm. Anal. Calorim. 143 (2) (2021) 1439–1454.
[84] M.H. Ahmadi, et al., A proposed model to predict thermal conductivity ratio of Al 2 O 3/EG nanofluid by applying least squares support vector machine (LSSVM) and genetic algorithm as a connectionist approach, J. Therm. Anal. Calorim. 135 (1) (2019) 271–281.
[85] Z. Tian, et al., Estimate the shear rate & apparent viscosity of multi-phased non-Newtonian hybrid nanofluids via new developed Support Vector Machine method coupled with sensitivity analysis, Physica A 535 (2019) 122456.
[86] S. Bhowmik, et al., Artificial intelligence based gene expression programming (GEP) model prediction of Diesel engine performances and exhaust emissions under Diesosenol fuel strategies, Fuel 235 (2019) 317–325.
[87] M. Umar, et al., A stochastic numerical computing heuristic of SIR nonlinear model based on dengue fever, Results Phys. 19 (2020) 103585.
[88] T. Szabó, O. Berkesi, I. Dékány, DRIFT study of deuterium-exchanged graphite oxide, Carbon 43 (15) (2005) 3186–3189.
[89] H. Zhang, et al., P25-graphene composite as a high performance photocatalyst, ACS Nano 4 (1) (2010) 380–386.
[90] A. Listanti, et al., Synthesis, structural and toxicity characters of nano-sized titanium dioxide/magnetite nanoparticles, IOP Conference Series: Materials Science and Engineering, IOP Publishing, 2019.
[91] V. Sumi, et al., Effect of rGO on Fe2O3–TiO2 composite incorporated NiP coating for boosting hydrogen evolution reaction in alkaline solution, Int. J. Hydrog. Energy 45 (4) (2020) 2460–2477.
[92] M.A. Baghchesara, et al., Improving the intrinsic properties of rGO sheets by S-doping and the effects of rGO improvements on the photocatalytic performance of Cu3Se2/rGO nanocomposites, Appl. Surf. Sci. 466 (2019) 401–410.
[93] W. Yu, H. Xie, A review on nanofluids: preparation, stability mechanisms, and applications, J. Nanomater. 2012 (2012) 435873.
[94] R. Kamatchi, S. Venkatachalapathy, B.A. Srinivas, Synthesis, stability, transport properties, and surface wettability of reduced graphene oxide/water nanofluids, Int. J. Therm. Sci. 97 (2015) 17–25.
[95] N.K. Cakmak, The impact of surfactants on the stability and thermal conductivity of graphene oxide de-ionized water nanofluids, J. Therm. Anal. Calorim. 139 (3) (2020) 1895–1902.
[96] W. Afzal, A.H. Mohammadi, D. Richon, Volumetric properties of mono-, di-, tri-, and polyethylene glycol aqueous solutions from (273.15 to 363.15) K: experimental measurements and correlations, J. Chem. Eng. Data 54 (4) (2009) 1254–1261.
[97] S.-R. Yan, et al., Rheological behavior of hybrid MWCNTs-TiO2/EG nanofluid: a comprehensive modeling and experimental study, J. Mol. Liq. (2020) 113058.
[98] M. Nayak, et al., Thermo-fluidic significance of non Newtonian fluid with hybrid nanostructures, Case Stud. Therm. Eng. (2021) 101092.
[99] L.R. de Oliveira, et al., Experimental study on the thermal conductivity and viscosity of ethylene glycol-based nanofluid containing diamond-silver hybrid material, Diam. Relat. Mater. 96 (2019) 216–230.
[100] M. Baratpour, et al., Effects of temperature and concentration on the viscosity of nanofluids made of single-wall carbon nanotubes in ethylene glycol, Int. Commun. Heat Mass Transfer 74 (2016) 108–113.
[101] D. Sawicka, J.T. Cieśliński, S. Smolen, A comparison of empirical correlations of viscosity and thermal conductivity of water-ethylene glycol-Al2O3 Nanofluids, Nanomaterials 10 (8) (2020) 1487.
[102] J. Yao, et al., A method of calculating the interaction energy between particles in minerals flotation, Math. Probl. Eng. 2016 (2016).
[103] I. Kazemi, M. Sefid, M. Afrand, A novel comparative experimental study on rheological behavior of mono & hybrid nanofluids concerned graphene and silica nanopowders: characterization, stability and viscosity measurements, Powder Technol. 366 (2020) 216–229.
[104] P.K. Namburu, et al., Viscosity of copper oxide nanoparticles dispersed in ethylene glycol and water mixture, Exp. Thermal Fluid Sci. 32 (2) (2007) 397–402.
[105] L.S. Sundar, et al., Viscosity of low volume concentrations of magnetic Fe3O4 nanoparticles dispersed in ethylene glycol and water mixture, Chem. Phys. Lett. 554 (2012) 236–242.
[106] L.S. Sundar, et al., Experimental investigation of the thermal transport properties of graphene oxide/Co3O4 hybrid nanofluids, Int. Commun. Heat Mass Transfer 84 (2017) 1–10.
[107] S.-h. Zhou, P. Guo, D.F. Stolle, Interaction model for “shelled particles” and small-strain modulus of granular materials, J. Appl. Mech. 85 (10) (2018) 101001.
[108] S. Bhowmik, et al., Artificial neural network prediction of diesel engine performance and emission fueled with diesel–kerosene–ethanol blends: a fuzzy-based optimization, J. Energy Resour. Technol. 139 (4) (2017).